


UAV-assisted cooperative NOMA and OFDM communication systems: Analysis and Optimization

Thuc Kieu-Xuan ^{1,†}, Anh Le-Thi ^{1,*} 

¹ Hanoi University of Industry; leanh@hau.edu.vn

* Correspondence: leanh@hau.edu.vn

[†] Hanoi University of Industry

[‡] These authors contributed equally to this work.

Abstract: Utilizing unmanned aerial vehicles (UAVs) to facilitate wireless communication has emerged as a viable and promising strategy aimed at enhancing both current and prospective wireless systems. This approach offers many advantages by establishing line-of-sight connections, optimizing operational efficiency, and enabling flexible deployment capabilities in various terrains. Thus, in this paper, we investigate UAV communication in a relaying network in which a UAV helps communication between a source and two destination users while flying to a location. To have a complete view of our proposed system, we consider both orthogonal multiple access as OFDM and non-orthogonal multiple access (NOMA) scenarios. Moreover, we apply successive convex optimization (SCO) and the Block-coordinate gradient descent (BCGD) for the sum-rate optimization problems to improve the system performance under constraints of total bandwidth and total power at the ground base station and UAV. The experimental results validate that the achievable secrecy rates are notably enhanced by using our proposed algorithms and show optimal trends for critical parameters, such as transmit powers, the flight trajectory and speed of UAV, and resource allocation of OFDM and NOMA.

Keywords: UAV-NOMA; UAV-OFDM; Successive convex optimization SCO; Sum data rate; Block-coordinate gradient descent BCGD.

1. Introduction

Over the past decade, unmanned aerial vehicles (UAVs), with their advantages of high mobility, low cost, and rapid deployment, have been used in diverse applications, including surveillance, rescue, cargo transport, and data collection in wireless sensor networks [1,2]. The research community is highly interested in the new emerging application of UAVs, that is, UAV-assisted wireless communication (UAVWC). Communication with the support of UAVs is an effective wireless network deployment solution for future communication models, specifically for 6G network systems [3]. Unlike terrestrial wireless networks where the wireless channel undergoes multi-path fading, UAVWC can provide line-of-sight connections to wireless devices by using aerial base stations; hence, UAVWC is expected to have a higher performance than existing terrestrial wireless systems. Moreover, the mobility and flexibility of UAVs allow UAVWCs to operate with broader coverage or in dangerous areas that require high deployment and maintenance costs of the base stations. To exploit the great benefits of UAVWC, many recent studies on wireless communication have done a lot of work to solve technical challenges and optimize the performance of UAVWC [4–6].

Furthermore, UAVs have gained extensive utilization within wireless sensor networks. Functioning as mobile access points or base stations, UAVs present a promising resolution to address the substantial storage demands prevalent in wireless sensor networks [2,7]. By facilitating UAV-assisted data aggregation from numerous sensor nodes equipped with wireless capabilities, the singular-antenna UAV empowers all sensor nodes within

Citation: Lastname, F.; Lastname, F.; Lastname, F. *Journal Not Specified* 2023, 1, 0. <https://doi.org/>

Received:

Revised:

Accepted:

Published:

Copyright: © 2023 by the authors. Submitted to *Journal Not Specified* for possible open access publication under the terms and conditions of the Creative Commons Attribution (CC BY) license (<https://creativecommons.org/licenses/by/4.0/>).

its coverage scope to transmit data. Consequently, these sensor nodes relay their collected information back to the UAV. Given the significant implications identified, there exists an imperative necessity to delve into research regarding the NOMA-UAV model. Thus, the model communication of the UAV-NOMA combination can significantly enhance the performance of wireless networks in a broader context and specifically contribute to advancing wireless sensor networks. Consequently, greater attention and scrutiny are warranted to explore the NOMA-UAV model's capabilities and implications comprehensively.

1.1. Related work

To optimize the performance of UAVWCs and exploit their benefits, recent studies on wireless communication have worked on overcoming various technical challenges. In [8], the authors examined and provided statistical models for an air-to-ground radio frequency (RF) channel in a dense urban environment, then air-to-ground RF statistical models for different conditions were investigated in [9]. These results allow network designers to make planning and performance easier evaluations for WN-aNWs. The studies of UAVWCs can be classified into two groups, one using UAVs as static aerial transceivers and another exploiting the mobility of UAVs, known as static and mobile UAVWCs, respectively. Moreover, in [10], the authors proposed a UAV deployment algorithm to minimize the number of UAVs needed to provide wireless coverage for a given area. In [11], the authors solved the up-link sum-rate maximization problem of a static wireless-powered UAVWC. Authors in [12] optimized the UAV's location and user association for UAV-assisted mobile networks with the goal of making the traffic loads of UAVs almost equal so that the networks can be stable. In [13], the authors considered a low-altitude aerial platform (LAP) for the urban environment and provided a mathematical model of the altitude and wireless coverage, allowing network designers to predict the optimum altitude of the static UAVWC.

NOMA has been evaluated as a potential solution for future networks, such as beyond fifth-generation (B5G) and sixth-generation (6G) networks, because its benefits can meet the new 6G performance requirement, especially for huge connectivity [14–17]. Thus, many publications have investigated the application of NOMA for UAV networks. Notably, authors in [18] outlined new opportunities and challenges with NOMA with the assistance of UAV in more significant rate regions, balanced performance between system throughput and fairness, and reduced delay. In [19], the authors evaluated the outage probability of UAV-aided non-orthogonal multiple access (NOMA) networks and uplink and downlink transmissions. In [20], the authors analyzed a UAV-aided device-to-device network's sum rate and average coverage probability for both static and mobile UAV scenarios. Moreover, authors in [21] investigated the delay-constrained performance analysis of a multi-antenna assisted multiuser NOMA-based spectrum sharing system and examined the sum effective rate for the downlink NOMA system. The work of [22] solved the problem of improving the secrecy performance in a UAV-assisted NOMA communication by jointly optimizing the UAV's trajectory and the transmit powers of legitimate users. A UAV-enabled space-air-ground integrated relay system applying the NOMA technique is presented in [23]. In this publication, authors summarized the UAV-ground NOMA communication into a max-min problem regarding UAV's energy efficiency. The use of artificial intelligence-driven UAV-NOMA to improve the quality of experiences of terrestrial multi-users is studied in the works [24,25]. Moreover, authors in [26] investigated the UAV in PD-NOMA with concurrent uplink transmission of the aerial user (AU) and terrestrial user (TU). To enhance the achievable data rate of both AU and TU, these authors developed an analytical framework to calculate the probability of rate coverage; the results showed that the min height of the AUE is contingent upon its distance from the BS as it follows a designated trajectory. This underscores the significance of accurately modeling the AUE trajectory within cellular-connected UAV systems. In [27], a heuristic algorithm and logarithmic approximation are applied to solve the problem of the total energy efficiency for UAV

Table 1. Summary of Related works

Previous works	System Models	Operation type	Primary findings
[18]	UAV – downlink NOMA, multiple terrestrial BSs, terrestrial users, aerial users	Ground-to-air connections: modeling, analyzing, and simulating via two metrics as coverage probability and average user rate	Balanced performance between system throughput and fairness, and reduced delay
[19]	UAV-uplink and downlink NOMA	Full-duplex and half-duplex schemes over Nakagami-m channel: modeling, analyzing, and simulating via main metric as outage probability (OP)	Exploiting the benefits of UAV as a relay, save bandwidth, improving the data transmission efficiency, deriving closed-form expressions for OP
[23]	UAV with phased-array antennas and NOMA scheme	Modeling, analyzing, optimizing and simulating via main metrics as energy efficiency (EE), trajectory, NOMA scheduling and NOMA power allocation	Their proposed system achieves the high EE, and NOMA was shown to outperform OMA in UAV EE.
[24]	UAV – NOMA with AI	Proposing some AI techniques can apply for UAV communication use NOMA to serve terrestrial mobile users: analysis and presentation	Main techniques as federated learning and reinforcement learning (RL) to address the intelligent task offloading and computing resource allocation
[25]	UAV with the uplink PD-NOMA and IRS	Multi IRS-UAV with ground BS and NOMA users: modeling, analyzing, optimizing and simulating	Two different RL based algorithms (DDQN and PPO) to minimize the average age-of information of user
[26]	UAV and power-domain aerial-terrestrial NOMA (uplink scheme)	Concurrent uplink transmission of the aerial user (AU) and terrestrial user (TU) in uplink to UAV: modeling, analytical framework, simulating via the probability of achievable data rate	Determining the minimum height that AU needs to fly, enhancing the quality of services and showing the importance of modeling AU trajectory in UAV system
[27]	UAV–downlink NOMA	Optimizing joint resource allocation and UAV trajectory to maximize the total EE: using heuristic algorithm and logarithmic approximation	Improving the total energy efficiency and transmit power allocation, data rate and computational complexity

communication in a downlink NOMA network. In summary, these related works exploring UAV facilitating NOMA communication are delineated in Table 1 and presented below.

1.2. Main contributions

As the analysis has shown above, specifically in Table 1, we see that the studies of the UAV flight trajectory, its influence, and transmitted power allocation to the NOMA-UAV network using mathematical methods are limited. Therefore, in this paper, we investigated a UAV relaying system including two users, a near user and a far user. The UAV's flight path is from a beginning position to an ending position, and it will assist in communication between a ground base station (GBS) and two destination users (DUs). Two multiple access techniques, orthogonal frequency division multiple access (OFDMA), in which the frequency resource is split for each user, and non-orthogonal multiple access (NOMA), in which the user's signals are transmitted on the same frequency resource with different power levels, are examined. The contributions of our work are encapsulated as follows:

- We consider non-convex problems of maximizing the system sum rate of the proposed UAVWC system under constrained conditions of the total bandwidth, total transmitted power at GBS and the UAV, and required sum rate of the far user for the NOMA and OFDMA scenarios;
- We propose algorithms using the SCO and BCGD techniques to identify excellent solutions for the proposed non-convex optimization problem of sum rate based on the UAV's trajectory and transmitted power. We show that our algorithms are guaranteed to coverage;
- Achievable simulated results Achieve simulated results reveal that the system sum data rate is remarkably ameliorated by applying our proposed algorithms and pointing out the optimal trends of critical system parameters with both NOMA and OFDM.

The remainder of this article is arranged as follows. The system model and preliminary results for OFDMA/NOMA-based UAV relaying (OFDMA/NOMA-UAVR) protocols are described in Section 2. The problem formulation and solution for the sum-rate maximization for OFDMA/NOMA-UAVR protocol are presented in Section 3. The overall algorithm and convergence analysis are presented in Section 4. The simulation results and discussions are presented in Section 5. Finally, the conclusions are presented in Section 6.

2. System model

120

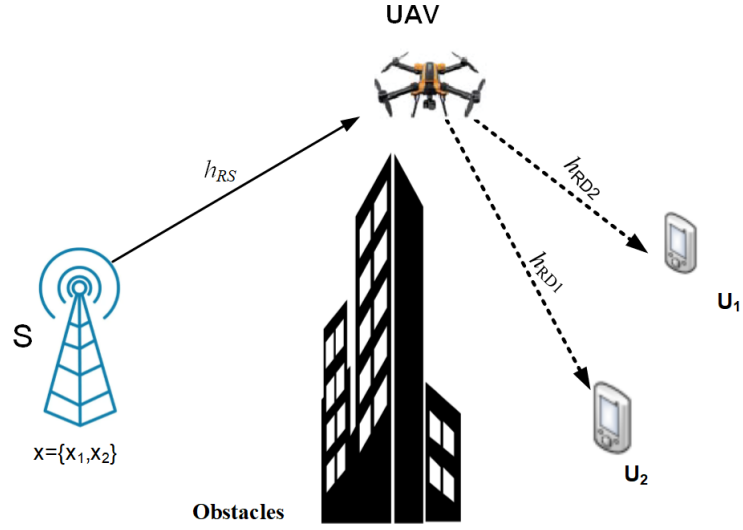


Figure 1. Proposed system model.

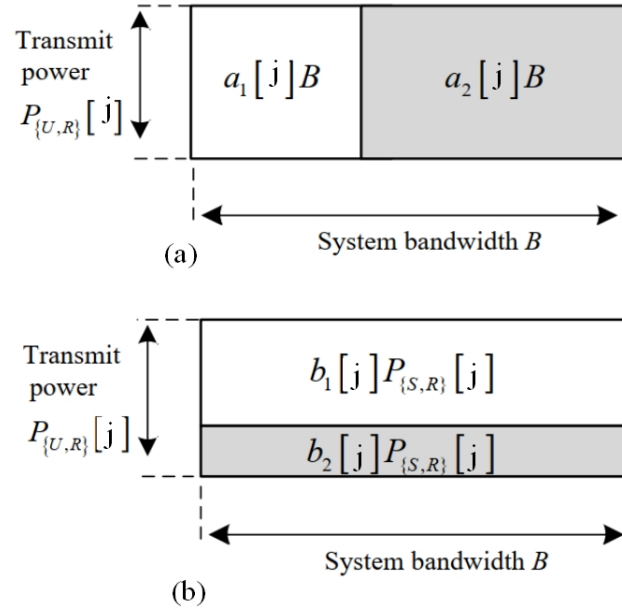


Figure 2. The communication models in each time slot for (a) the OFDMA-UAVR protocol and (b) the NOMA-UAVR protocol.

We consider a UAV relaying system, as illustrated in Fig. 1, in which a UAV, R , flies at a fixed altitude H from an initial location $\mathbf{R}_I(R_{Ix}, R_{Iy})$ to a final location $\mathbf{R}_F(R_{Fx}, R_{Fy})$, and helps a source S communicate with a closer user U_1 and a further user U_2 . S , U_1 , and U_2 are terrestrial single-antenna nodes. R uses the decode-and-forward (DF) protocol to assist the communication. We assume that: (i) there is no direct link between S and users because of obstacles; (ii) the Relay's operation is in a length of time T ; (iii) the UAV taking off and landing are not considered, and we concentrate on the UAV operation period and altitude H ; and (iv) T is split into N equal time slots $\delta_j = \delta_0 \triangleq \frac{T}{N}$, $1 \leq j \leq N$, where δ_0 is adequately small such that the position of UAV can be determined as a constant during δ_j . Finally, in this paper, system variables for this system model are summarized in Table 2.

121
122
123
124
125
126
127
128
129
130

Table 2. Summary of system variables

No.	Symbol	Description
1	P	Transmit power
2	B	Bandwidth
3	H	Fixed altitude
4	R_I	Initial location
5	R_F	Final location
6	T	Length of time
7	N	Time slots
8	h_X	Channel gain
9	$a_i[j]$	Bandwidth allocation factor in OFDM
10	R	Instantaneous rate
11	R^{th}	required sum-rate
12	n_X	The additive white Gaussian noise
13	$b_i[j]$	The power allocation factor of NOMA
14	$P_{Y,\Sigma}$	The power budget
15	$P_{Y,\max}$	Maximum transmit power

The horizontal positions of S , U_1 , U_2 , and R during δ_n are represented by $\mathbf{S}(S_x, S_y)$, $\mathbf{U}_1(U_{1x}, U_{1y})$, $\mathbf{U}_2(U_{2x}, U_{2y})$, and $\mathbf{w}[j](x_j, y_j)$, $1 \leq j \leq j$, respectively. The channel gain from R to a ground source node X , $X \in \{S, U_1, U_2\}$, during δ_j is given by:

$$|h_{RX}[j]|^2 = \frac{\beta_0}{H^2 + \|\mathbf{w}[j] - \mathbf{X}\|^2}. \quad (1)$$

here, β_0 is the channel gain at a $d_0 = 1$ (m).

In the following, we present the transmission in each time slot for the OFDMA-based UAV relaying (OFDMA-UAVR) and NOMA-based UAV relaying (NOMA-UAVR) protocols in the half-duplex mode. Thus, the communication for each time slot is split into two sub-time slots, as shown in Fig. 2.

2.1. OFDMA-based UAV relaying protocol

S transmits the signals in the initial sub-time slot within δ_j that are $s_1[j]$ and $s_2[j]$, with the power $P_S[j]$ on the bandwidths $a_1[j]B$ and $a_2[j]B$, respectively, where B is the system bandwidth, $a_i[j]$, $i \in \{1, 2\}$ is the bandwidth allocation factor of OFDMA and satisfies both $a_1[j] + a_2[j] = 1$ and $a_i[j] > a_{\min}$ with $0 < a_{\min} < 0.5$ is the smallest values of $a_j[i]$. The received signal and instantaneous rate at R are given by

$$y_{R,s_i}^{\text{ofdma}}[j] = \sqrt{P_S[j]} h_{SR}[j] s_i[j] + n_{R,i}[j], \quad (2)$$

$$R_{R,s_i}^{\text{ofdma}}[j] = a_i[j] \log_2 \left(1 + \frac{P_S[j] |h_{RS}[j]|^2}{N_0} \right), \quad (3)$$

here $n_{R,i}[j] \sim \mathcal{CN}(0, N_0)$ is the additive white Gaussian noise (AWGN) at R .

During the following sub-time slot within δ_j , Relay node will forward $s_1[j]$ and $s_2[j]$ to U_1 and U_2 , respectively, on their corresponding bandwidths. The received signal and instantaneous rate at U_i are given by

$$y_{U_i,s_i}^{\text{ofdma}}[j] = \sqrt{P_R[j]} h_{RU_i}[j] s_i[j] + n_{U_i}[j], \quad (4)$$

$$R_{U_i,s_i}^{\text{ofdma}}[j] = a_i[j] \log_2 \left(1 + \frac{P_R[j] |h_{RU_i}[j]|^2}{N_0} \right), \quad (5)$$

here, $P_R[j]$ is the transmitted power of R node and $n_{U_i}[j] \sim \mathcal{CN}(0, N_0)$ is AWGN at U_i .

Due to R node acts as the DF relay, the end-to-end instantaneous rate of $s_i[j]$ for guaranteeing successful decoding at U_i is given by

$$R_{s_i}^{\text{ofdma}} = \min(R_{R,s_i}^{\text{ofdma}}[j], R_{U_i,s_i}^{\text{ofdma}}[j]). \quad (6)$$

2.2. NOMA-based UAV relaying protocol

In the initial sub-time slot within δ_n , S broadcasts the superimposed signals, $s_1[j]$ and $s_2[j]$, with the powers $b_1[j]P_S[j]$ and $b_2[j]P_S[j]$, respectively, on bandwidth B where $b_i[j], i \in \{1, 2\}$ is the power allocation factor of NOMA and satisfies both $b_1[j] + b_2[j] = 1$ and $b_i[j] > b_{\min}$ with $0 < b_{\min} < 0.5$ is the smallest values of $b_i[j]$. The received signal at R node can be expressed as

$$y_{R,s_1}^{\text{noma}}[j] = \sqrt{P_S[j]}h_{RS}[j] \left(\sqrt{b_1[j]}s_1[j] + \sqrt{b_2[j]}s_2[j] \right) + n_R[j]. \quad (7)$$

Using SIC (successive interference cancellation), R decodes $s_2[j]$ first and then eliminates $s_2[j]$ from the received signal before decoding $s_1[j]$. The instantaneous rates of $s_1[j]$ and $s_2[j]$ for guaranteeing successful decoding at R are given by

$$R_{R,s_1}^{\text{noma}}[j] = \log_2 \left(1 + \frac{b_1[j]P_S[j]|h_{SR}[j]|^2}{N_0} \right), \quad (8)$$

$$R_{R,s_2}^{\text{noma}}[j] = \log_2 \left(1 + \frac{b_2[j]P_S[j]|h_{SR}[j]|^2}{b_1[j]P_S[j]|h_{SR}[j]|^2 + N_0} \right). \quad (9)$$

In the second sub-interval slot within δ_n , R node will forward $s_1[j]$ and $s_2[j]$ with the powers $a_1[j]P_R[j]$ and $a_2[j]P_R[j]$, respectively, on bandwidth B . The received signal at U_i is given by

$$y_{U_i}^{\text{noma}}[j] = \sqrt{P_R[j]}h_{RU_i}[j] \left(\sqrt{b_1[j]}s_1[j] + \sqrt{b_2[j]}s_2[j] \right) + n_{U_i}[j]. \quad (10)$$

At U_1 , SIC is employed to decode $s_2[j]$ before decoding $s_1[j]$. The instantaneous rates of $s_1[j]$ and $s_2[j]$ for guaranteeing successful decoding at U_1 are given by

$$R_{U_1,s_1}^{\text{noma}}[j] = \log_2 \left(1 + \frac{b_1[j]P_R[j]|h_{RU_1}[j]|^2}{N_0} \right), \quad (11)$$

$$R_{U_1,s_2}^{\text{noma}}[j] = \log_2 \left(1 + \frac{b_2[j]P_R[j]|h_{RU_1}[j]|^2}{b_1[j]P_R[j]|h_{RU_1}[j]|^2 + N_0} \right). \quad (12)$$

The instantaneous rate of $s_2[j]$ at U_2 is given by

$$R_{U_2,s_2}^{\text{noma}}[j] = \log_2 \left(1 + \frac{b_2[j]P_R[j]|h_{RU_2}[j]|^2}{b_1[j]P_R[j]|h_{RU_2}[j]|^2 + N_0} \right). \quad (13)$$

Since R is the DF relay, the end-to-end instantaneous rate of $s_i[j]$ for guaranteeing successful decoding at U_i is given by

$$R_{s_i}^{\text{noma}} = \min(R_{R,s_i}^{\text{noma}}[j], R_{U_i,s_i}^{\text{noma}}[j]). \quad (14)$$

3. Analysis of Sum-Rate optimization problem

Within this section, we define the problem of maximizing the sum rate of the proposed system under the constraint of the required sum rate at U_2 , $R_{U_2}^{\text{th}}$, for both OFDMA-UAVR and OFDMA-UAVR protocols. Letting $P_{Y,\Sigma}$ and $P_{Y,\max}$ denote the power budget and maximum transmit power during δ_n of node $Y \in \{S, R\}$, we have the following inequalities

$$\sum_{j=1}^N P_S[j] \leq P_{S,\Sigma}, \quad (15)$$

$$P_S[j] \leq P_{S,\max}, 1 \leq j \leq j, \quad (16)$$

$$\sum_{j=1}^N P_R[j] \leq P_{R,\Sigma}, \quad (17)$$

$$P_R[j] \leq P_{R,\max}, 1 \leq j \leq j. \quad (18)$$

With above assumptions in Section 2, the constraints of the UAV trajectory or of R are expressed as

$$\mathbf{w}[1] = \mathbf{R}_I, \quad (19)$$

$$\|\mathbf{w}[j+1] - \mathbf{w}[j]\| \leq V_{\max}\delta_0, 1 \leq j \leq j-1, \quad (20)$$

$$\|\mathbf{R}_F - \mathbf{w}[j]\| \leq V_{\max}\delta_0. \quad (21)$$

$$(P1) \quad \max_{\mathbf{P}_S, \mathbf{P}_R, \mathbf{a}, \mathbf{W}} \sum_{j=1}^N \left(a_1[j] \min(R_{R,s_1}^{\text{odfma}}[j], R_{U_1,s_1}^{\text{odfma}}[j]) + a_2[j] \min(R_{R,s_2}^{\text{odfma}}[j], R_{U_2,s_2}^{\text{odfma}}[j]) \right), \quad (22a)$$

$$\text{s.t.} \quad a_{\min} \leq a_1[j] \leq 1 - a_{\min}, \quad 1 \leq j \leq j, \quad (22b)$$

$$a_1[j] + a_2[j] = 1, \quad 1 \leq j \leq j, \quad (22c)$$

$$\sum_{j=1}^N \left(a_2[j] \min(R_{R,s_2}^{\text{odfma}}[j], R_{U_2,s_2}^{\text{odfma}}[j]) \right) \geq R_{U_2}^{\text{th}}, \quad (22d)$$

$$(15 - 21).$$

$$(P2) \quad \max_{\mathbf{P}_S, \mathbf{P}_R, \mathbf{b}, \mathbf{W}} \sum_{j=1}^N \left(\min(R_{R,s_1}^{\text{noma}}[j], R_{U_1,s_1}^{\text{noma}}[j]) + \min(R_{R,s_2}^{\text{noma}}[j], R_{U_2,s_1}^{\text{noma}}[j]) \right), \quad (23a)$$

$$\text{s.t.} \quad b_{\min} \leq b_1[j] \leq 1 - b_{\min}, 1 \leq j \leq j, \quad (23b)$$

$$b_1[j] + b_2[j] = 1, 1 \leq j \leq j, \quad (23c)$$

$$R_{U_2,x_2}^{\text{noma}} \leq R_{U_1,x_2}^{\text{noma}}, \quad (23d)$$

$$\sum_{j=1}^N \left(\min(R_{R,s_2}^{\text{noma}}[j], R_{U_2,s_1}^{\text{noma}}[j]) \right) \geq R_{U_2}^{\text{th}}, \quad (23e)$$

$$(15 - 21).$$

Next, letting $\mathbf{P}_S \triangleq [P_S[1], \dots, P_S[j]]$, $\mathbf{P}_R \triangleq [P_R[1], \dots, P_R[j]]$, $\mathbf{a} \triangleq [a_1[1], \dots, a_1[j]]$, $\mathbf{b} \triangleq [b_1[1], \dots, b_1[j]]$ and $\mathbf{W} \triangleq [\mathbf{w}[1], \dots, \mathbf{w}[j]]$, the issues related to maximizing the sum-rate of our proposed system for both the OFDMA-UAVR and NOMA-UAVR protocols are respectively formulated as in (22) and (23) shown at the top of the next page.

For the NOMA-UAVR protocol, the SIC of U_1 must decode $s_2[j]$ before trying to detect the signal $s_1[j]$; hence, constraint in equation (23d) is the condition for successful decoding $s_2[j]$ at U_1 that allows the SIC at U_1 to operate correctly.

Since the objective functions in (22a) and (23a) are neither convex nor concave, (P1) and (P2) is not convex optimizing problems. Subsequently, we propose alternative solutions for these problems using the BCGD and SCO approaches. In particular, we apply the BCGD approach to optimize individual variable blocks of (P1) and (P2) while maintaining the other variable blocks unchanged. For a given resource allocation factor \mathbf{a} (or \mathbf{b}) and transmit powers $\mathbf{P} \triangleq \{\mathbf{P}_S, \mathbf{P}_R\}$, we optimize the trajectory of R , \mathbf{W} , (defined as (P1.1) and (P2.1) for the OFDMA-UAVR and NOMA-UAVR protocols, respectively). For a given UAV's trajectory \mathbf{W} and \mathbf{a} (or \mathbf{b}), we optimize the transmit powers \mathbf{P} (defined as (P1.2) and (P2.2) for the OFDMA-UAVR and NOMA-UAVR protocols, respectively). Finally, for a given \mathbf{W} and \mathbf{P} , we optimize \mathbf{a} for the OFDMA-UAVR protocol (defined as (P1.3)) and \mathbf{b} for the NOMA-UAVR protocol (defined as (P2.3)). The non-convex objective functions are addressed by applying the SCO method. Ultimately, we introduce the comprehensive algorithms and prove the convergence behaviour of these proposed methods.

3.1. UAV Trajectory Optimization

In this subsection, we use the SCO method to optimize the trajectory of R for the OFDMA-UAVR and NOMA-UAVR protocols.

3.1.1. OFDMA-based UAV relaying protocol

Substituting (1) into (3) and (5) yields

$$R_{R,s_i}^{\text{ofdma}}[j] = a_i[j] \log_2 \left(1 + \frac{\mathbb{A}_1^{\text{ofdma}}[j]}{H^2 + \|\mathbf{w}[j] - \mathbf{S}\|^2} \right), \quad (24)$$

$$R_{U_i,s_i}^{\text{ofdma}}[j] = a_i[j] \log_2 \left(1 + \frac{\mathbb{A}_2^{\text{ofdma}}[j]}{H^2 + \|\mathbf{w}[j] - \mathbf{U}_i\|^2} \right), \quad (25)$$

where $\mathbb{A}_1^{\text{ofdma}}[j] = \frac{P_S[j]\beta_0}{N_0}$ and $\mathbb{A}_2^{\text{ofdma}}[j] = \frac{P_R[j]\beta_0}{N_0}$.

It is seen that although (24) and (25) lack convexity concerning $\mathbf{w}[j]$, they exhibit convexity in relation to $\|\mathbf{w}[j] - \mathbf{S}\|^2$ and $\|\mathbf{w}[j] - \mathbf{U}_i\|^2$, respectively. This attribute allows us to derive lower bounds for $R_{R,s_i}^{\text{ofdma}}[j]$ and $R_{U_i,s_i}^{\text{ofdma}}[j]$ that are convex with respect to $\mathbf{w}[j]$. Specifically, at a given point $\mathbf{W}^l \triangleq [\mathbf{w}^l[1], \dots, \mathbf{w}^l[j]]$ (we assume that \mathbf{W}^l is the optimal UAV's flight trajectory obtained after the l -th iteration), the following lower bounds can be obtained using the first-order Taylor expansion [17].

$$\begin{aligned} R_{R,s_i}^{\text{ofdma}}[j] &\geq \hat{R}_{R,s_i}^{\text{ofdma}}[j] \\ &= a_i[j] \left(\mathcal{A}_1^{\text{ofdma}}[j] \|\mathbf{w}[j] - \mathbf{S}\|^2 + \mathcal{B}_1^{\text{ofdma}}[j] \right), \end{aligned} \quad (26)$$

$$\begin{aligned} R_{U_i,s_i}^{\text{ofdma}}[j] &\geq \hat{R}_{U_i,s_i}^{\text{ofdma}}[j] \\ &= a_i[j] \left(\mathcal{A}_{i+1}^{\text{ofdma}}[j] \|\mathbf{w}[j] - \mathbf{U}_i\|^2 + \mathcal{B}_{i+1}^{\text{ofdma}}[j] \right), \end{aligned} \quad (27)$$

where $\mathcal{A}_1^{\text{ofdma}}[j]$, $\mathcal{A}_{i+1}^{\text{ofdma}}[j]$, $\mathcal{B}_1^{\text{ofdma}}[j]$ and $\mathcal{B}_{i+1}^{\text{ofdma}}[j]$ are given by

$$\begin{aligned} \mathcal{A}_1^{\text{ofdma}}[j] &= \left(\mathbb{A}_1^{\text{ofdma}}[j] + H^2 + \|\mathbf{w}^l[j] - \mathbf{S}\|^2 \right)^{-1} \\ &\quad - \left(H^2 + \|\mathbf{w}^l[j] - \mathbf{S}\|^2 \right)^{-1}, \end{aligned} \quad (28a)$$

$$\begin{aligned} \mathcal{A}_{i+1}^{\text{ofdma}}[j] &= \left(\mathbb{A}_2^{\text{ofdma}}[j] + H^2 + \|\mathbf{w}^l[j] - \mathbf{U}_i\|^2 \right)^{-1} \\ &\quad - \left(H^2 + \|\mathbf{w}^l[j] - \mathbf{U}_i\|^2 \right)^{-1}, \end{aligned} \quad (28b)$$

$$\begin{aligned} \mathcal{B}_1^{\text{ofdma}}[j] &= \ln \left(1 + \frac{\mathbb{A}_1^{\text{ofdma}}[j]}{H^2 + \|\mathbf{w}^l[j] - \mathbf{S}\|^2} \right) \\ &\quad - \mathcal{A}_1^{\text{ofdma}}[j] \|\mathbf{w}^l[j] - \mathbf{S}\|^2, \end{aligned} \quad (28c)$$

$$\begin{aligned} \mathcal{B}_{i+1}^{\text{ofdma}}[j] &= \ln \left(1 + \frac{\mathbb{A}_2^{\text{ofdma}}[j]}{H^2 + \|\mathbf{w}^l[j] - \mathbf{U}_i\|^2} \right) \\ &\quad - \mathcal{A}_{i+1}^{\text{ofdma}}[j] \|\mathbf{w}^l[j] - \mathbf{U}_i\|^2. \end{aligned} \quad (28d)$$

Using (26) and (27), at any given \mathbf{a} , \mathbf{P} and \mathbf{W}^l , (P1) is approximated by (P1.1) (or (29)) shown at the top of the next page. It is seen that (P1.1) is a convex optimization

$$(P1.1) \quad \max_{\mathbf{w}} \frac{1}{\log(2)} \sum_{j=1}^N \left(\begin{aligned} &a_1[j] \min \left(\mathcal{A}_1^{\text{ofdma}}[j] \|\mathbf{w}[j] - \mathbf{S}\|^2 + \mathcal{B}_1^{\text{ofdma}}[j], \right. \\ &\quad \left. + a_2[j] \min \left(\mathcal{A}_2^{\text{ofdma}}[j] \|\mathbf{w}[j] - \mathbf{U}_1\|^2 + \mathcal{B}_2^{\text{ofdma}}[j], \right. \right. \\ &\quad \left. \left. + a_3[j] \min \left(\mathcal{A}_3^{\text{ofdma}}[j] \|\mathbf{w}[j] - \mathbf{U}_2\|^2 + \mathcal{B}_3^{\text{ofdma}}[j] \right) \right) \right) \end{aligned} \right), \quad (29a)$$

$$\begin{aligned} \text{s.t.} \quad & \frac{1}{\ln(2)} \sum_{j=1}^N \left(a_2[j] \min \left(\mathcal{A}_1^{\text{ofdma}}[j] \|\mathbf{w}[j] - \mathbf{S}\|^2 + \mathcal{B}_1^{\text{ofdma}}[j], \right. \right. \\ & \quad \left. \left. \mathcal{A}_3^{\text{ofdma}}[j] \|\mathbf{w}[j] - \mathbf{U}_2\|^2 + \mathcal{B}_3^{\text{ofdma}}[j] \right) \right) \geq R_{U_2}^{\text{th}}, \end{aligned} \quad (29b)$$

(19 – 21).

problem that can be efficiently solved by standard convex optimization solvers (such as CVX implemented in Matlab).

3.1.2. NOMA-based UAV relaying protocol

Substituting (1) into (8), (9), (11), (12) and (13) and after some manipulations, we have

$$R_{R,s_1}^{\text{noma}} = \log_2 \left(1 + \frac{\mathbb{A}_1^{\text{noma}}[j]}{H^2 + \|\mathbf{w}[j] - \mathbf{S}\|^2} \right), \quad (30)$$

$$R_{R,s_2}^{\text{noma}} = \log_2 \left(1 + \frac{\mathbb{A}_0^{\text{noma}}[j] \mathbb{A}_1^{\text{noma}}[j]}{\mathbb{A}_1^{\text{noma}}[j] + H^2 + \|\mathbf{w}[j] - \mathbf{S}\|^2} \right), \quad (31)$$

$$R_{U_1,s_1}^{\text{noma}} = \log_2 \left(1 + \frac{\mathbb{A}_2^{\text{noma}}[j]}{H^2 + \|\mathbf{w}[j] - \mathbf{U}_1\|^2} \right), \quad (32)$$

$$R_{U_1,s_2}^{\text{noma}} = \log_2 \left(1 + \frac{\mathbb{A}_0^{\text{noma}}[j] \mathbb{A}_2^{\text{noma}}[j]}{\mathbb{A}_2^{\text{noma}}[j] + H^2 + \|\mathbf{w}[j] - \mathbf{U}_1\|^2} \right), \quad (33)$$

$$R_{U_2,s_2}^{\text{noma}} = \log_2 \left(1 + \frac{\mathbb{A}_0^{\text{noma}}[j] \mathbb{A}_2^{\text{noma}}[j]}{\mathbb{A}_2^{\text{noma}}[j] + H^2 + \|\mathbf{w}[j] - \mathbf{U}_2\|^2} \right), \quad (34)$$

where $\mathbb{A}_0^{\text{noma}}[j] = \frac{b_2[j]}{b_1[j]}$, $\mathbb{A}_1^{\text{noma}}[j] = \frac{b_1[j]P_S[j]\beta_0}{N_0}$ and $\mathbb{A}_2^{\text{noma}}[j] = \frac{b_1[j]P_R[j]\beta_0}{N_0}$.

Following the similar approach as in 3.1.1, we can obtain the following inequalities using the first-order Taylor expansion.

$$\begin{aligned} R_{R,s_k}^{\text{noma}}[j] &\geq \hat{R}_{R,s_k}^{\text{noma}}[j] \\ &\triangleq \mathcal{A}_k^{\text{noma}}[j] \|\mathbf{w}[j] - \mathbf{S}\|^2 + \mathcal{B}_k^{\text{noma}}[j], \end{aligned} \quad (35)$$

$$\begin{aligned} R_{U_k,s_k}^{\text{noma}}[j] &\geq \hat{R}_{U_k,s_k}^{\text{noma}}[j] \\ &\triangleq \mathcal{A}_{k+2}^{\text{noma}}[j] \|\mathbf{w}[j] - \mathbf{U}_k\|^2 + \mathcal{B}_{k+2}^{\text{noma}}[j], \end{aligned} \quad (36)$$

where $\mathcal{A}_1^{\text{noma}}[j]$, $\mathcal{A}_2^{\text{noma}}[j]$, $\mathcal{A}_3^{\text{noma}}[j]$, $\mathcal{A}_4^{\text{noma}}[j]$, $\mathcal{B}_1^{\text{noma}}[j]$, $\mathcal{B}_2^{\text{noma}}[j]$, $\mathcal{B}_3^{\text{noma}}[j]$ and $\mathcal{B}_4^{\text{noma}}[j]$ are given in (37) shown at the top of the next page.

$$\mathcal{A}_1^{\text{noma}}[j] = \left(\|\mathbf{w}^l[j] - \mathbf{S}\|^2 + \mathbb{A}_1^{\text{noma}}[j] + H^2 \right)^{-1} - \left(\|\mathbf{w}^l[j] - \mathbf{S}\|^2 + H^2 \right)^{-1}, \quad (37a)$$

$$\mathcal{A}_2^{\text{noma}}[j] = \left(\|\mathbf{w}^l[j] - \mathbf{S}\|^2 + (\mathbb{A}_0^{\text{noma}} + 1)\mathbb{A}_1^{\text{noma}} + H^2 \right)^{-1} - \left(\|\mathbf{w}^l[j] - \mathbf{S}\|^2 + \mathbb{A}_1^{\text{noma}} + H^2 \right)^{-1}, \quad (37b)$$

$$\mathcal{A}_3^{\text{noma}}[j] = \left(\|\mathbf{w}^l[j] - \mathbf{U}_1\|^2 + \mathbb{A}_2^{\text{noma}} + H^2 \right)^{-1} - \left(\|\mathbf{w}^l[j] - \mathbf{U}_1\|^2 + H^2 \right)^{-1}, \quad (37c)$$

$$\mathcal{A}_4^{\text{noma}}[j] = \left(\|\mathbf{w}^l[j] - \mathbf{U}_2\|^2 + (\mathbb{A}_0^{\text{noma}} + 1)\mathbb{A}_2^{\text{noma}} + H^2 \right)^{-1} - \left(\|\mathbf{w}^l[j] - \mathbf{U}_2\|^2 + \mathbb{A}_2^{\text{noma}} + H^2 \right)^{-1}, \quad (37d)$$

$$\mathcal{B}_1^{\text{noma}}[j] = \log \left(1 + \frac{\mathbb{A}_1^{\text{noma}}}{H^2 + \|\mathbf{w}^l[j] - \mathbf{S}\|^2} \right) - \mathcal{A}_1 \|\mathbf{w}^l[j] - \mathbf{S}\|^2, \quad (37e)$$

$$\mathcal{B}_2^{\text{noma}}[j] = \log \left(1 + \frac{\mathbb{A}_0^{\text{noma}} \mathbb{A}_1^{\text{noma}}}{\mathbb{A}_1^{\text{noma}} + H^2 + \|\mathbf{w}^l[j] - \mathbf{S}\|^2} \right) - \mathcal{A}_2 \|\mathbf{w}^l[j] - \mathbf{S}\|^2, \quad (37f)$$

$$\mathcal{B}_3^{\text{noma}}[j] = \log \left(1 + \frac{\mathbb{A}_2^{\text{noma}}}{H^2 + \|\mathbf{w}^l[j] - \mathbf{U}_1\|^2} \right) - \mathcal{A}_3 \|\mathbf{w}^l[j] - \mathbf{U}_1\|^2, \quad (37g)$$

$$\mathcal{B}_4^{\text{noma}}[j] = \log \left(1 + \frac{\mathbb{A}_0^{\text{noma}} \mathbb{A}_2^{\text{noma}}}{\mathbb{A}_2^{\text{noma}} + H^2 + \|\mathbf{w}^l[j] - \mathbf{U}_2\|^2} \right) - \mathcal{A}_4^{\text{noma}}[j] \|\mathbf{w}^l[j] - \mathbf{U}_2\|^2. \quad (37h)$$

$$(P2.1) \quad \max_{\mathbf{w}} \frac{1}{\ln(2)} \sum_{j=1}^N \left(\min \left(\mathcal{A}_1^{\text{noma}} \|\mathbf{w}[j] - \mathbf{S}\|^2 + \mathcal{B}_1^{\text{noma}}, \mathcal{A}_3^{\text{noma}} \|\mathbf{w}[j] - \mathbf{U}_1\|^2 + \mathcal{B}_3^{\text{noma}} \right) + \min \left(\mathcal{A}_2^{\text{noma}} \|\mathbf{w}[j] - \mathbf{S}\|^2 + \mathcal{B}_2^{\text{noma}}, \mathcal{A}_4^{\text{noma}} \|\mathbf{w}[j] - \mathbf{U}_2\|^2 + \mathcal{B}_4^{\text{noma}} \right) \right), \quad (40a)$$

$$\text{s.t.} \quad \frac{1}{\ln(2)} \sum_{j=1}^N \left(\min \left(\mathcal{A}_2^{\text{noma}} \|\mathbf{w}[j] - \mathbf{S}\|^2 + \mathcal{B}_2^{\text{noma}}, \mathcal{A}_4^{\text{noma}} \|\mathbf{w}[j] - \mathbf{U}_2\|^2 + \mathcal{B}_4^{\text{noma}} \right) \right) \geq R_{U_2}^{\text{th}}, \quad (40b)$$

(19 – 21, 39).

Next, using (33) and (34), Constraint (23d) can be rewritten as

$$\|\mathbf{w}[j] - \mathbf{U}_1\|^2 \leq \|\mathbf{w}[j] - \mathbf{U}_2\|^2. \quad (38)$$

It is seen that (38) is not a convex constraint. Since the right-hand side of (38) is convex with respect to $\mathbf{w}[j]$, (38) can be rewritten applying the first-order Taylor expansion as follows.

$$\begin{aligned} \|\mathbf{w}[j] - \mathbf{U}_1\|^2 &\leq (\mathbf{w}^l[j] - \mathbf{U}_2)^\top (\mathbf{w}[j] - \mathbf{U}_2) \\ &\quad - \|\mathbf{w}^l[j] - \mathbf{U}_2\|^2. \end{aligned} \quad (39)$$

Using (35), (36) and (39), for any given \mathbf{a} , \mathbf{P} and \mathbf{W}^l , (P2) is approximated by (P2.1) (or (40)) shown at the top of the next page. It is seen that (P2.1) is a convex optimization problem, and we can apply standard convex optimization techniques to address this efficiently.

3.2. Transmit Power Optimization

In this subsection, we optimize the transmit powers of S and R for the OFDMA-UAVR and NOMA-UAVR protocols.

3.2.1. OFDMA-based UAV relaying protocol

Substituting (6) into (22), at a given \mathbf{a} and \mathbf{W}^l , (P1) can be expressed as (P1.2) (or (41)) shown at the top of the next page where $\mathbb{B}_1^{\text{ofdma}} = \frac{|h_{RS}[j]|^2}{N_0}$, $\mathbb{B}_2^{\text{ofdma}} = \frac{|h_{RU_1}[j]|^2}{N_0}$ and

$$(P1.2) \quad \max_{\mathbf{P}} \frac{1}{\ln(2)} \sum_{j=1}^N \left(a_1[j] \min \left(\log_2 \left(1 + \mathbb{B}_1^{\text{ofdma}} P_S[j] \right), \log_2 \left(1 + \mathbb{B}_2^{\text{ofdma}} P_R[j] \right) \right) + a_2[j] \min \left(\log_2 \left(1 + \mathbb{B}_1^{\text{ofdma}} P_S[j] \right), \log_2 \left(1 + \mathbb{B}_3^{\text{ofdma}} P_R[j] \right) \right) \right), \quad (41a)$$

$$\text{s.t.} \quad \frac{1}{\ln(2)} \sum_{j=1}^N \left(a_2[j] \min \left(\log_2 \left(1 + \mathbb{B}_1^{\text{ofdma}} P_S[j] \right), \log_2 \left(1 + \mathbb{B}_3^{\text{ofdma}} P_R[j] \right) \right) \right) \geq R_{x_2}^{\text{th}}, \quad (41b)$$

(15 – 18),

$$\mathbb{B}_3^{\text{ofdma}} = \frac{|h_{RU_2}[j]|^2}{N_0}.$$

It is seen that (P1.2) represents a convex optimization problem amenable to efficient resolution using standard convex optimization solvers.

3.2.2. NOMA-based UAV relaying protocol

For any given \mathbf{a} and \mathbf{W}^l , (9) and (13) can be rewritten as

$$R_{R,s_2}^{\text{noma}} = \log_2(1 + \mathbb{B}_4^{\text{noma}} P_S[j]) - \log_2(1 + \mathbb{B}_1^{\text{noma}} P_S[j]), \quad (42)$$

$$R_{U_2,s_2}^{\text{noma}} = \log_2(1 + \mathbb{B}_5^{\text{noma}} P_R[j]) - \log_2(1 + \mathbb{B}_2^{\text{noma}} P_R[j]), \quad (43)$$

where $\mathbb{B}_1^{\text{noma}} = \frac{b_1[j]|h_{SR}[j]|^2}{N_0}$, $\mathbb{B}_2^{\text{noma}} = \frac{b_1[j]|h_{RU_2}[j]|^2}{N_0}$, $\mathbb{B}_4^{\text{noma}} = \frac{|h_{SR}[j]|^2}{N_0}$ and $\mathbb{B}_5^{\text{noma}} = \frac{|h_{RU_2}[j]|^2}{N_0}$.

Let $\mathbf{P}_S^l \triangleq \{\mathbf{P}_S^l, \mathbf{P}_R^l\}$, where $\mathbf{P}_S^l \triangleq [P_S^l[1], \dots, P_S^l[j]]$ and $\mathbf{P}_R^l \triangleq [P_R^l[1], \dots, P_R^l[j]]$ are the optimal transmit powers of S and R , respectively, obtained after the l -th iteration. The application of the first-order Taylor expansion allows us to derive the following inequalities.

$$\begin{aligned} R_{R,s_2}^{\text{noma}} &\geq \hat{R}_{R,s_2}^{\text{noma}} \\ &= \frac{1}{\ln(2)} (\ln(1 + \mathbb{B}_4^{\text{noma}} P_S[j]) - \mathcal{C}_{1a}^{\text{no}} P_S[j] - \mathcal{C}_{1b}^{\text{no}}), \end{aligned} \quad (44)$$

$$\begin{aligned} R_{U_2,s_2}^{\text{noma}} &\geq \hat{R}_{U_2,s_2}^{\text{noma}} \\ &= \frac{1}{\ln(2)} (\ln(1 + \mathbb{B}_5^{\text{noma}} P_R[j]) - \mathcal{C}_{2a}^{\text{no}} P_R[j] - \mathcal{C}_{2b}^{\text{no}}), \end{aligned} \quad (45)$$

where $\mathcal{C}_{1a}^{\text{noma}}, \mathcal{C}_{1b}^{\text{noma}}, \mathcal{C}_{2a}^{\text{noma}}$ and $\mathcal{C}_{2b}^{\text{noma}}$ are given by

$$\mathcal{C}_{1a}^{\text{noma}} = \frac{\mathbb{B}_1^{\text{noma}}}{1 + \mathbb{B}_1^{\text{noma}} P_S^l[j]}, \quad (46a)$$

$$\mathcal{C}_{1b}^{\text{noma}} = \ln(1 + \mathbb{B}_1^{\text{noma}} P_S^l[j]) - \mathcal{C}_{1a}^{\text{noma}} P_S^l[j], \quad (46b)$$

$$\mathcal{C}_{2a}^{\text{noma}} = \frac{\mathbb{B}_2^{\text{noma}}}{1 + \mathbb{B}_2^{\text{noma}} P_R^l[j]}, \quad (46c)$$

$$\mathcal{C}_{2b}^{\text{noma}} = \ln(1 + \mathbb{B}_2^{\text{noma}} P_R^l[j]) - \mathcal{C}_{2a}^{\text{noma}} P_R^l[j]. \quad (46d)$$

Substituting (8), (11), (44) and (45) into (23), (P2) can be approximated by (P2.2) (or (47)) shown at the top of the next page where $\mathbb{B}_3^{\text{no}} = \frac{b_1[j]|h_{RU_1}[j]|^2}{N_0}$. It is seen that (P2.2) is a convex

$$(P2.2) \quad \max_{\mathbf{P}} \frac{1}{\ln(2)} \sum_{j=1}^N \left(\min(\ln(1 + \mathbb{B}_1^{\text{noma}} P_S[j]), \ln(1 + \mathbb{B}_3^{\text{noma}} P_R[j])) \right. \\ \left. + \min \left(\frac{\ln(1 + \mathbb{B}_4^{\text{noma}} P_S[j]) - (\mathcal{C}_{1a}^{\text{noma}} P_S[j] + \mathcal{C}_{1b}^{\text{noma}})}{\ln(1 + \mathbb{B}_5^{\text{noma}} P_R[j]) - (\mathcal{C}_{2a}^{\text{noma}} P_R[j] + \mathcal{C}_{2b}^{\text{noma}})} \right) \right), \quad (47a)$$

$$\text{s.t.} \quad \frac{1}{\ln(2)} \sum_{j=1}^N \left(\min \left(\frac{\ln(1 + \mathbb{B}_4^{\text{noma}} P_S[j]) - (\mathcal{C}_{1a}^{\text{noma}} P_S[j] + \mathcal{C}_{1b}^{\text{noma}})}{\ln(1 + \mathbb{B}_5^{\text{noma}} P_R[j]) - (\mathcal{C}_{2a}^{\text{noma}} P_R[j] + \mathcal{C}_{2b}^{\text{noma}})} \right) \right) \geq R_{x_2}^{\text{th}}, \quad (47b)$$

(15 – 18).

problem that can be efficiently addressed by using conventional convex optimization solvers.

3.3. Optimizing the Resource Allocation

In this subsection, we optimize the bandwidth allocation factor \mathbf{a} and power allocation factor \mathbf{b} for the OFDMA-UAVR and NOMA-UAVR protocols.

$$(P1.3) \quad \max_{\mathbf{a}} \sum_{j=1}^N \left(a_1[j] \min(R_{R,x_1}^{\text{odfma}}[j], R_{U_1,x_1}^{\text{odfma}}[j]) + a_2[j] \min(R_{R,x_2}^{\text{odfma}}[j], R_{U_2,x_2}^{\text{odfma}}[j]) \right), \quad (48a)$$

$$\text{s.t.} \quad \sum_{j=1}^N \left(a_2[j] \min(R_{R,x_2}^{\text{odfma}}[j], R_{U_2,x_2}^{\text{odfma}}[j]) \right) \geq R_{U_2}^{\text{th}}, \quad (48b)$$

(22b – 22c).

3.3.1. OFDMA-based UAV relaying protocol

For any given \mathbf{P} and \mathbf{W} , (P1) can be rewritten as (P1.3) (or (48)) shown at the top of the next page. It is seen that (P1.3) is a convex optimization problem that can be efficiently addressed by using conventional convex optimization solvers.

3.3.2. NOMA-based UAV relaying protocol

For any given \mathbf{P} and \mathbf{W} , (9) and (13) are rewritten as

$$R_{R,s_2}^{\text{noma}} = \log_2 \left(\frac{1 + \mathbb{C}_1^{\text{noma}}}{b_1[j] + \mathbb{C}_1^{\text{noma}}} \right) \geq R_{R,s_2}^{\text{noma}} \\ \triangleq \log_2(1 + \mathbb{C}_1^{\text{noma}}) - \mathcal{D}_{1a}b_1[j] - \mathcal{D}_{1b}, \quad (49)$$

$$R_{U_2,s_2}^{\text{noma}} = \log_2 \left(\frac{1 + \mathbb{C}_3^{\text{noma}}}{b_1[j] + \mathbb{C}_3^{\text{noma}}} \right) \geq R_{U_2,s_2}^{\text{noma}} \\ \triangleq \log_2(1 + \mathbb{C}_3^{\text{noma}}) - \mathcal{D}_{2a}b_1[j] - \mathcal{D}_{2b}, \quad (50)$$

where $\mathbb{C}_1^{\text{noma}} = \frac{N_0}{P_S[j]|h_{SR}[j]|^2}$, $\mathbb{C}_2^{\text{noma}} = \frac{N_0}{P_R[j]|h_{RU_1}[j]|^2}$ and $\mathbb{C}_3^{\text{noma}} = \frac{N_0}{P_R[j]|h_{RU_2}[j]|^2}$.

Substituting (8), (11), (49) and (50) into (23), (P2) can be approximated by (P2.3) (or (51)) shown at the top of the next page. We can see that (P2.3) is also a convex optimization

$$(P2.3) \quad \max_{\mathbf{b}} \frac{1}{\ln(2)} \sum_{j=1}^N \left(\min \left(\ln \left(1 + \frac{b_1[j]}{\mathbb{C}_1^{\text{noma}}} \right), \ln \left(1 + \frac{b_1[j]}{\mathbb{C}_2^{\text{noma}}} \right) \right) \right. \\ \left. + \min \left(\ln \left(1 + \frac{\mathbb{C}_1^{\text{noma}}}{b_1[j] + \mathbb{C}_1^{\text{noma}}} \right) - \mathcal{D}_{1a}b_1[j] - \mathcal{D}_{1b}, \right. \right. \\ \left. \left. \ln \left(1 + \frac{\mathbb{C}_3^{\text{noma}}}{b_1[j] + \mathbb{C}_3^{\text{noma}}} \right) - \mathcal{D}_{2a}b_1[j] - \mathcal{D}_{2b} \right) \right), \quad (51a)$$

$$\text{s.t.} \quad \frac{1}{\ln(2)} \sum_{j=1}^N \left(\min \left(\ln \left(1 + \frac{\mathbb{C}_1^{\text{noma}}}{b_1[j] + \mathbb{C}_1^{\text{noma}}} \right) - \mathcal{D}_{1a}b_1[j] - \mathcal{D}_{1b}, \right. \right. \\ \left. \left. \ln \left(1 + \frac{\mathbb{C}_3^{\text{noma}}}{b_1[j] + \mathbb{C}_3^{\text{noma}}} \right) - \mathcal{D}_{2a}b_1[j] - \mathcal{D}_{2b} \right) \right) \geq R_{U_2}^{\text{th}}, \quad (51b)$$

(23b).

problem that can be ably addressed by standard convex optimization methods.

4. Proposed Comprehensive Algorithm

4.1. Proposed algorithm

In this part, we introduce the comprehensive algorithms for obtaining efficient approximate solutions for (P1) and (P2) through the utilization of BCGD method. We also present the outcomes of suboptimal problems, namely (P1.1), (P1.2), (P1.3), (P2.1), (P2.2) and (P2.3). More precisely, the optimization variables consist of three blocks $\{\mathbf{W}, \mathbf{P}, \boldsymbol{\theta}\}$ where $\boldsymbol{\theta}$ is the resource allocation factor, i.e., $\boldsymbol{\theta} \equiv \mathbf{a}$ for the OFDMA-UAVR protocol and $\boldsymbol{\theta} \equiv \mathbf{b}$ for the NOMA-UAVR protocol. Each block of $\{\mathbf{W}, \mathbf{P}, \boldsymbol{\theta}\}$ is optimized via addressing (P1.1), (P1.2) and (P1.3) (or (P2.1), (P2.2) and (P2.3)) correspondingly while fixing the values of the rest blocks. The obtained solution after optimizing each block is updated to $\{\mathbf{P}, \mathbf{W}, \boldsymbol{\theta}\}$

Table 3. Algorithm 1: The Sum-Rate Maximization Algorithm for OFDMA/NOMA-UAVR Protocols.

1.	Initialize $\{\mathbf{W}^0, \mathbf{P}^0, \theta^0\}$. Let $l = 0$.
2.	Repeat
3.	With given $\{\mathbf{P}^l, \theta^l\}$, solve (P1.1) or P(2.1) to find and then update the optimal UAV's trajectory to \mathbf{W}^{l+1} .
4.	With given $\{\mathbf{W}^{l+1}, \theta^l\}$, solve (P1.2) or P(2.2) to find and then update the optimal transmit powers to \mathbf{P}^{l+1} .
5.	With given $\{\mathbf{W}^{l+1}, \mathbf{P}^{l+1}\}$, solve (P1.3) or P(2.3) to find and then update the optimal PS ratio to θ^{l+1} .
6.	Update $l = l + 1$.
7.	Until The fractional increase of the objective value is below a small threshold ε .

correspondingly. This process is repeated until a certain condition is met. The details of this algorithm are summarized in Algorithm 1. 270
271

In the following, we show the convergence of Algorithm 1. Let $\eta(\mathbf{W}, \mathbf{P}, \theta)$, $\eta_{\mathbf{W}}^{\text{lb},l}(\mathbf{W}, \mathbf{P}, \theta)$, $\eta_{\mathbf{P}}^{\text{lb},l}(\mathbf{W}, \mathbf{P}, \theta)$ and $\eta_{\theta}^{\text{lb},l}(\mathbf{W}, \mathbf{P}, \theta)$ be respectively the objective functions of either (P1), (P1.1), (P1.2) and (P1.3) for the OFDMA-UAVR protocol or of (P2), (P2.1), (P2.2) and (P2.3) for the NOMA-UAVR protocol. First, at any provided point $\{\mathbf{P}^l, \mathbf{W}^l, \theta^l\}$, the subsequent inequalities are derived through the execution of Step (3) in Algorithm 1: 272
273
274
275
276

$$\eta(\mathbf{W}^l, \mathbf{P}^l, \theta^l) \stackrel{(a)}{=} \eta_{\mathbf{W}}^{\text{lb},l}(\mathbf{W}^l, \mathbf{P}^l, \theta^l), \quad (52a)$$

$$\stackrel{(b)}{\leq} \eta_{\mathbf{W}}^{\text{lb},l}(\mathbf{W}^{l+1}, \mathbf{P}^l, \theta^l), \quad (52b)$$

$$\stackrel{(c)}{\leq} \eta(\mathbf{W}^{l+1}, \mathbf{P}^l, \theta^l), \quad (52c)$$

where (a) holds, since the first-order Taylor expansions at (26, 27, 35, 36) are performed at the point $\{\mathbf{W}^l, \mathbf{P}^l, \theta^l\}$; (b) holds, since \mathbf{W}^{l+1} is the optimal solution of (P1.1) (or P(2.1)); and (c) holds, since the objective functions of (P1.1) and (P2.1) are the lower bounds of those of (P1) and (P2), respectively. 277
278
279
280

Using similar explanations for (P1.2), (P1.3), (P2.2), and (P2.3), the inequalities in (53) and (54) can be proven as follows. Then, at any provided point $\{\mathbf{W}^{l+1}, \mathbf{P}^l, \theta^l\}$, we can get the following inequalities via Step (4) of Algorithm 1: 281
282
283

$$\eta(\mathbf{W}^{l+1}, \mathbf{P}^l, \theta^l) = \eta_{\mathbf{P}}^{\text{lb},l}(\mathbf{W}^{l+1}, \mathbf{P}^l, \theta^l), \quad (53a)$$

$$\leq \eta_{\mathbf{P}}^{\text{lb},l}(\mathbf{W}^{l+1}, \mathbf{P}^{l+1}, \theta^l), \quad (53b)$$

$$\leq \eta(\mathbf{W}^{l+1}, \mathbf{P}^{l+1}, \theta^l). \quad (53c)$$

Next, at any provided point $\{\mathbf{W}^{l+1}, \mathbf{P}^{l+1}, \boldsymbol{\theta}^l\}$, we also get the following inequalities via Step (5) of Algorithm 1:

$$\eta(\mathbf{W}^{l+1}, \mathbf{P}^{l+1}, \boldsymbol{\theta}^l) = \eta_{\boldsymbol{\theta}}^{\text{lb},l}(\mathbf{W}^{l+1}, \mathbf{P}^{l+1}, \boldsymbol{\theta}^l), \quad (54a)$$

$$\leq \eta_{\boldsymbol{\theta}}^{\text{lb},l}(\mathbf{W}^{l+1}, \mathbf{P}^{l+1}, \boldsymbol{\theta}^{l+1}), \quad (54b)$$

$$\leq \eta(\mathbf{W}^{l+1}, \mathbf{P}^{l+1}, \boldsymbol{\theta}^{l+1}). \quad (54c)$$

Finally, we have

$$\eta(\mathbf{P}^l, \mathbf{W}^l, \boldsymbol{\theta}^l) \leq \eta(\mathbf{W}^{l+1}, \mathbf{P}^{l+1}, \boldsymbol{\theta}^{l+1}). \quad (55)$$

This observation reveals that the objective values of (P1) and (P2) are non-decreasing trend throughout iterations. Furthermore, the optimized values of (P1) and (P2) are finite, ensuring the guaranteed convergence of Algorithm 1.

4.2. Initialization scheme

In this part, we introduce the Algorithm 2 which aims to discover an attainable initial variable block $\{\mathbf{W}^0, \mathbf{P}^0, \boldsymbol{\theta}^0\}$ for Algorithm 1. Due to the constraint of the sum data rate of U_2 , the key concept behind Algorithm 2 that is maximizing the sum-rate of U_2 for the OFDMA-UAVR and NOMA-UAVR protocols, respectively defined as (P3) and (P4). Note that the values of $a_2[n]$ and $b_2[n]$ are set at their highest values; hence, $\boldsymbol{\theta}_{\text{InitS}} = (1 - a_{\min})[\underbrace{1, \dots, 1}_{N \text{ elements}}]^\top$

for the OFDMA-UAVR protocol and $\boldsymbol{\theta}_{\text{InitS}} = (1 - b_{\min})[\underbrace{1, \dots, 1}_{N \text{ elements}}]^\top$ for the NOMA-UAVR protocol. If the maximum achievable sum rate with Algorithm 2 surpasses that of $R_{U_2}^{\text{th}}$, the current optimal flight trajectory and transmit powers are \mathbf{W}^0 and \mathbf{P}^0 , respectively; otherwise, (P1) and (P2) are infeasible optimization problems. By modifying (P1) and (P2), we can obtain (P3) and (P4) as

$$(P3) \quad \max_{\mathbf{P}_S, \mathbf{P}_R, \mathbf{W}} \sum_{j=1}^N \left((1 - a_{\min}) \min(R_{R,x_2}^{\text{odfma}}[j], R_{U_2,x_2}^{\text{odfma}}[j]) \right), \quad (56a)$$

$$\text{s.t.} \quad (15 - 21). \quad (56b)$$

$$(P4) \quad \max_{\mathbf{P}_S, \mathbf{P}_R, \mathbf{W}} \sum_{j=1}^N \left(\min(R_{R,x_2}^{\text{noma}}[j], R_{U_2,x_1}^{\text{noma}}[j]) \right), \quad (57a)$$

$$\text{s.t.} \quad (15 - 21, 23d). \quad (57b)$$

Similarly, the problems of (P3) and (P4) are not convex optimization. Therefore, we have introduced alternative solutions for (P3) and (P4) employing the BCGD and SCO approaches. Concretely, the optimization variables consist of two blocks $\{\mathbf{W}, \mathbf{P}\}$. Subsequently, the BCGD technique is employed to perform optimization for each of these variable blocks within the context of (P3) (or (P4)), while holding the other variable blocks constant. With transmit powers $\mathbf{P} \triangleq \{\mathbf{P}_S, \mathbf{P}_R\}$, we optimize \mathbf{W} (defined as (P3.1) and (P4.1) for the OFDMA-UAVR and NOMA-UAVR protocols, respectively); and for a given UAV's trajectory \mathbf{W} , we optimize \mathbf{P} (defined as (P3.2) and (P4.2) for the OFDMA-UAVR and NOMA-UAVR protocols, respectively). The result achieved through the optimization of each block is then adjusted in accordance with \mathbf{W}, \mathbf{P} . This iteration continues until a specific

$$(P3.1) \quad \max_{\mathbf{W}} \frac{1 - a_{\min}}{\log(2)} \sum_{j=1}^N \left(\min \left(\mathcal{A}_1^{\text{odfma}}[j] \|\mathbf{w}[j] - \mathbf{S}\|^2 + \mathcal{B}_1^{\text{odfma}}[j], \mathcal{A}_3^{\text{odfma}}[j] \|\mathbf{w}[j] - \mathbf{U}_2\|^2 + \mathcal{B}_3^{\text{odfma}}[j] \right) \right), \quad (58a)$$

$$\text{s.t.} \quad (19 - 21). \quad (58b)$$

$$(P4.1) \quad \max_{\mathbf{W}} \frac{1}{\ln(2)} \sum_{j=1}^N \left(\min \left(\mathcal{A}_2^{\text{noma}} \|\mathbf{w}[j] - \mathbf{S}\|^2 + \mathcal{B}_2^{\text{noma}}, \mathcal{A}_4^{\text{noma}} \|\mathbf{w}[j] - \mathbf{U}_2\|^2 + \mathcal{B}_4^{\text{noma}} \right) \right), \quad (59a)$$

$$\text{s.t.} \quad (19 - 21, 39). \quad (59b)$$

$$(P3.2) \quad \max_{\mathbf{P}} \frac{1 - a_{\min}}{\ln(2)} \sum_{j=1}^N \left(\min \left(\log_2 \left(1 + \mathbb{B}_1^{\text{odfma}} P_S[j] \right), \log_2 \left(1 + \mathbb{B}_3^{\text{odfma}} P_R[j] \right) \right) \right), \quad (60a)$$

$$\text{s.t.} \quad (15 - 18). \quad (60b)$$

$$(P4.2) \quad \max_{\mathbf{P}} \frac{1}{\ln(2)} \sum_{j=1}^N \left(\min \left(\frac{\ln(1 + \mathbb{B}_4^{\text{noma}} P_S[j]) - (\mathcal{C}_{1a}^{\text{no}} P_S[j] + \mathcal{C}_{1b}^{\text{no}})}{\ln(1 + \mathbb{B}_5^{\text{noma}} P_R[j]) - (\mathcal{C}_{2a}^{\text{no}} P_R[j] + \mathcal{C}_{2b}^{\text{no}})} \right) \right), \quad (61a)$$

$$\text{s.t.} \quad (15 - 18). \quad (61b)$$

criterion is satisfied. Furthermore, the objective functions with non-convex characteristics are addressed by applying the SCO technique. 313

By applying (29) and (40), the optimization problems of (P3.1) and (P4.1) at any given \mathbf{P} and \mathbf{W}^l are respectively given by (58) and (59), shown in the top of the next page. 314

Using (41, 47), the optimization problems of (P3.2) and (P4.2) at any given \mathbf{P}^l and \mathbf{W} are respectively given by (60) and (61), shown in the top of the next page. 315

Ultimately, a summary of Algorithm 2 can be located in Table 2, where L_{\max} is the utmost limit of iterations. 316

Algorithm 2 begins with an initial flight path of the UAV, which consists of a straight line connecting points \mathbf{R}_I and \mathbf{R}_F and maintains a constant velocity of V_0 , where $V_0 = \frac{|\mathbf{R}_I - \mathbf{R}_F|}{T}$. Additionally, the initial transmission power settings are established $\mathbf{P}_{S, \text{InitS}}^0[j] = P_{S, \Sigma}/N$ and $\mathbf{P}_{R, \text{InitS}}^0[j] = P_{R, \Sigma}/N$. 317

5. SIMULATION RESULTS 320

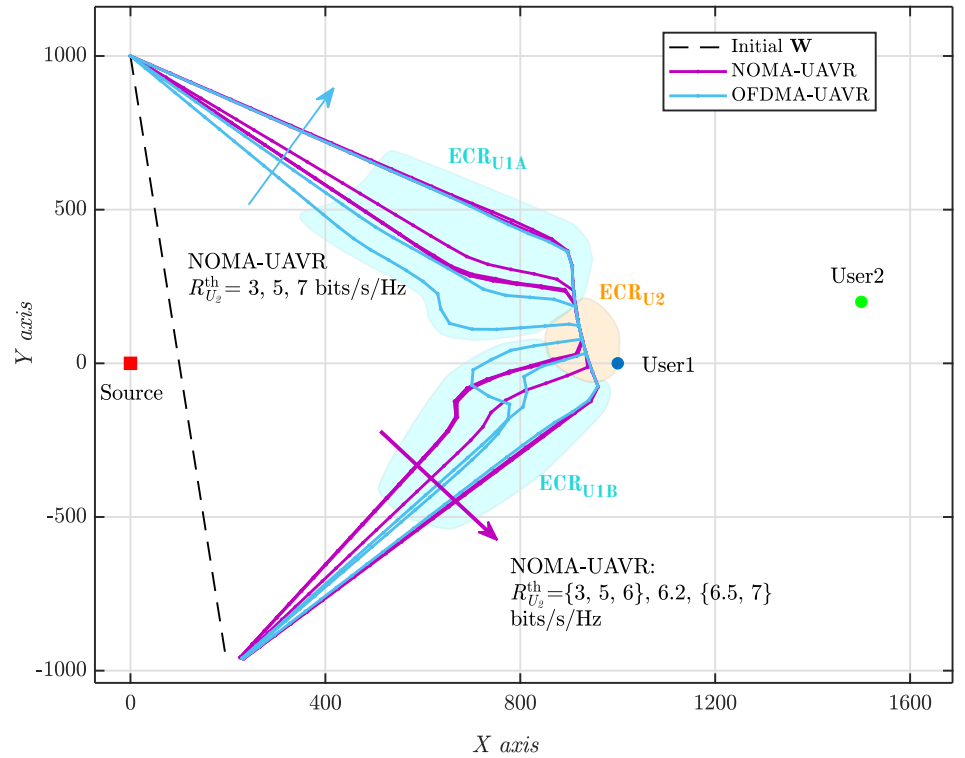
This section presents numerical findings to validate the effectiveness of our proposed optimization algorithms. The system parameters are set-up in our simulations as: $T = 300$ (s), $N = 60$, $\beta_0 = 1$, $\frac{P_{S, \max}}{N_0} = \frac{P_{R, \max}}{N_0} = 30$ (dB), $P_{S, \Sigma} = \eta_S P_{S, \max} N$, $P_{R, \Sigma} = \eta_R P_{R, \max} N$, $\eta_S = 0.25$, $\eta_R = 0.1$, $V_{\max} = 20$ (m/s), $H = 70$ (meters) and $N_0 = 1$. The measured coordinates in meters for \mathbf{S} , \mathbf{U}_1 , \mathbf{U}_2 , \mathbf{R}_I and \mathbf{R}_F are respectively set as $[0, 0]$, $[1000, 0]$, $[1500, 200]$, $[0, 1000]$ and $[200, -1000]$. 321

5.1. UAV's flight trajectory and velocity analysis 322

In Figs. 3 and 4, we investigate the optimum flight path and velocity of R obtained using the proposed algorithms. The trajectory of R is separated into three phases. At the initial phase ($n \leq 13$), the positions of R are far from the source and users; this leads to low efficient communication. For this reason, during the initial phase, R almost does not forward any information to users and it flies quickly to efficient communication regions (ECRs) where it can assist the commutation at higher data rates. At the second 323

Table 4. Algorithm 2: The Initialization Scheme for Algorithm 1

1.	Initialize $\{\mathbf{W}_{\text{InitS}}^0, \mathbf{P}_{\text{InitS}}^0\}$. Let $l = 0$.
2.	Repeat
3.	With given $\{\mathbf{W}_{\text{InitS}}^l, \mathbf{P}_{\text{InitS}}^l\}$, solve (P3.1) or P(4.1) to find and then update the optimal UAV's trajectory to $\mathbf{W}_{\text{InitS}}^{l+1}$.
4.	With given $\{\mathbf{W}_{\text{InitS}}^{l+1}, \mathbf{P}_{\text{InitS}}^l\}$, solve (P3.2) or P(4.2) to find and then update the optimal transmit powers to $\mathbf{P}_{\text{InitS}}^{l+1}$.
5.	Update $l = l + 1$.
6.	Until The objective value η_{InitS} is higher than $R_{U_2}^{\text{th}}$ or $l \geq L_{\text{max}}$.
7.	If $\eta_{\text{InitS}} \geq R_{U_2}^{\text{th}}$
8.	$\{\mathbf{W}^0, \mathbf{P}^0, \theta^0\} \leftarrow \{\mathbf{W}_{\text{InitS}}^{l+1}, \mathbf{P}_{\text{InitS}}^{l+1}, \theta_{\text{InitS}}\}$
9.	Else
10.	(P1) and (P2) are infeasible optimization problems.
11.	End if

**Figure 3.** The optimal flight path for the UAV under varying $C_{U_2}^{\text{th}}$ values.

phase, the efficient-communication phase (ECP), ($14 \leq j \leq 48$), R operates over the two
specific ECRs, the ECR_{U1} , $\text{ECR}_{U1} = \{\text{ECR}_{U1a}, \text{ECR}_{U1b}\}$, for providing the good $S - U_1$
communication and ECR_{U2} for providing the good $S - U_2$ communication. ECR_{U1} and
 ECR_{U2} are illustrated as in Fig. 3. Depending on the configuration of the system, the size of
ECRs can be larger or smaller. It is seen that the ECRs are between the source and users that
agree with the assessment for the optimum location of the static relay in the conventional
relaying systems. As shown in Fig. 4, R spends a duration (around $28 \leq j \leq 32$) to stay
at ECR_{U2} to guarantee the required sum-rate of U_2 , $R_{U_2}^{\text{th}}$, and also to maximize the system

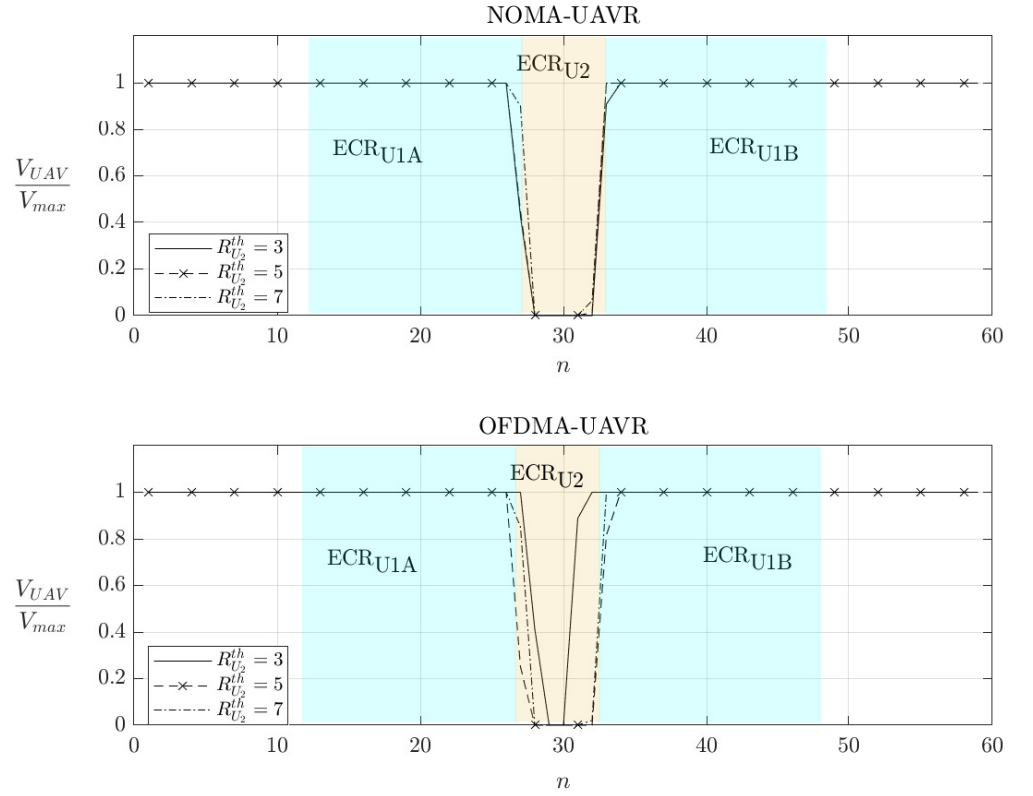
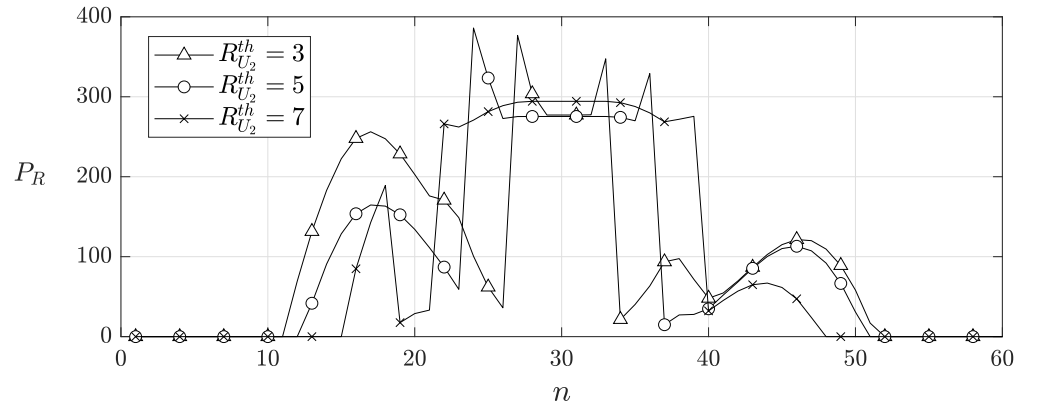
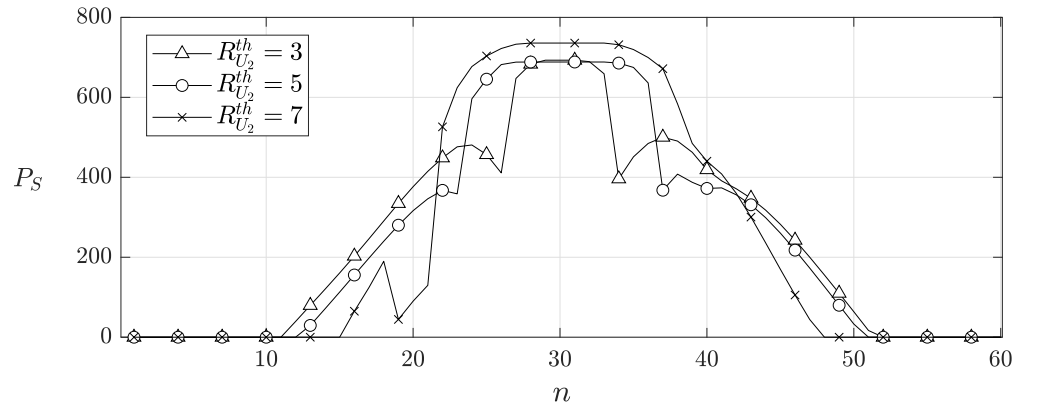


Figure 4. The optimal velocity of the UAV under varying $R_{U_2}^{\text{th}}$ values.

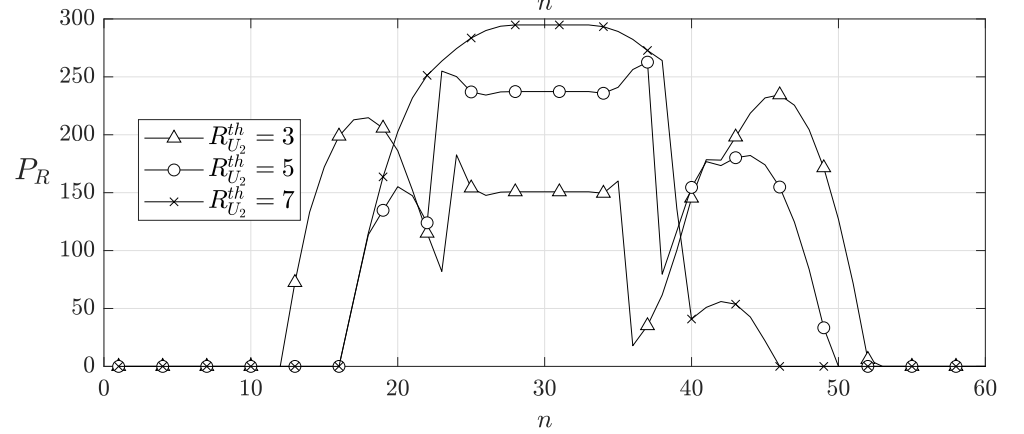
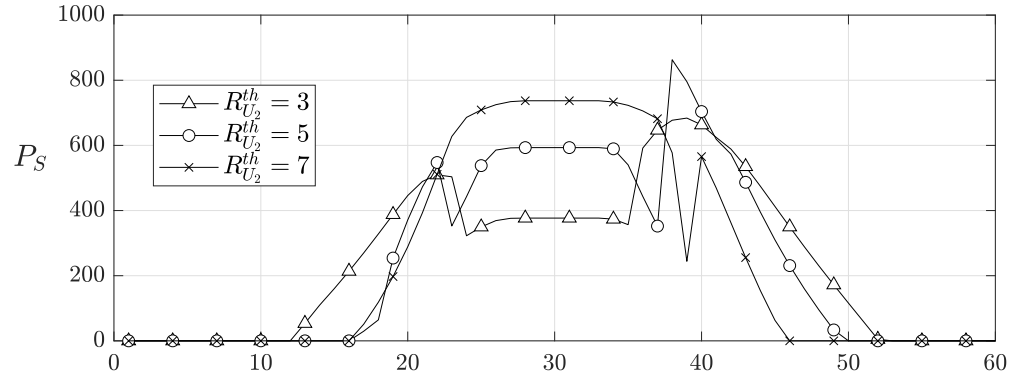
sum-rate. When U_2 requires more data, i.e., $R_{U_2}^{\text{th}}$ increases, R tends to spend more time at ECR_{U_2} . This can be confirmed using the results for velocity for the case of $R_{U_2}^{\text{th}} = 7$ (bits/s/Hz). For the NOMA-UAVR protocol, the trajectory significantly changes as $R_{U_2}^{\text{th}}$ increases from 6 to 6.5 (bits/s/Hz), otherwise it almost does not change. For the OFDMA-UAVR protocol, the trajectory substantially changes with the increase of $R_{U_2}^{\text{th}}$. For high values for $R_{U_2}^{\text{th}}$, R flies with a similar trajectory in both NOMA-UAVR and OFDMA-UAVR protocols. At the final phase ($n \geq 49$), R stops forwarding the information to users and quickly flies from ECR_{U_1} and/or ECR_{U_2} to the final location.

5.2. Transmission powers and resource allocation analysis

In Figs.5 and 6, we present the optimal transmitted powers and resource allocation elements (i.e., **a** and **b**) obtained using the proposed algorithms. In these figures, we focus on the patterns in the transmission power levels, **a** and **b**) during the ECP ($14 \leq j \leq 48$). Particularly, these trends are separated into three sub-phases. During the first sub-phase of the ECP, the transmit powers increase as R flies closer to ECR_{U_1a} , then reach a peak and decrease as R flies far away from ECR_{U_1a} to transit to ECR_{U_2} . Next, during the second sub-phase of the ECP, the transmits powers increase again as R flies toward to ECR_{U_2} , then they slightly vary as R flies in ECR_{U_2} , and finally, they decrease as R flies far away from ECR_{U_2} and transits to ECR_{U_1b} . The trends of the transmit powers in the last sub-phase of the ECP are the opposite trends for that during the first sub-phase of ECP. Moreover, the trends observed at low values of $R_{U_2}^{\text{th}}$ (e.g. $R_{U_2}^{\text{th}} < 7$) are more obvious than those observed at high values of (e.g. $R_{U_2}^{\text{th}} = 7$ (bits/s/Hz)). As shown in Fig. 6, the general trend of **a**₁ (or **b**₁) is receiving high values as R flies near ECR_{U_1} and low values as R flies near ECR_{U_2} . Similarly, we can also explain the trend of **a**₁ (or **b**₁) using the effects of the trajectory of R , ECR_{U_1} and ECR_{U_2} on the instantaneous rates at U_1 and U_2 .



(a)



(b)

Figure 5. The transmit powers (P_R, P_S) of the (a) OFDMA-UAVR and (b) NOMA-UAVR protocols with different values of $R_{U_2}^{th}$.

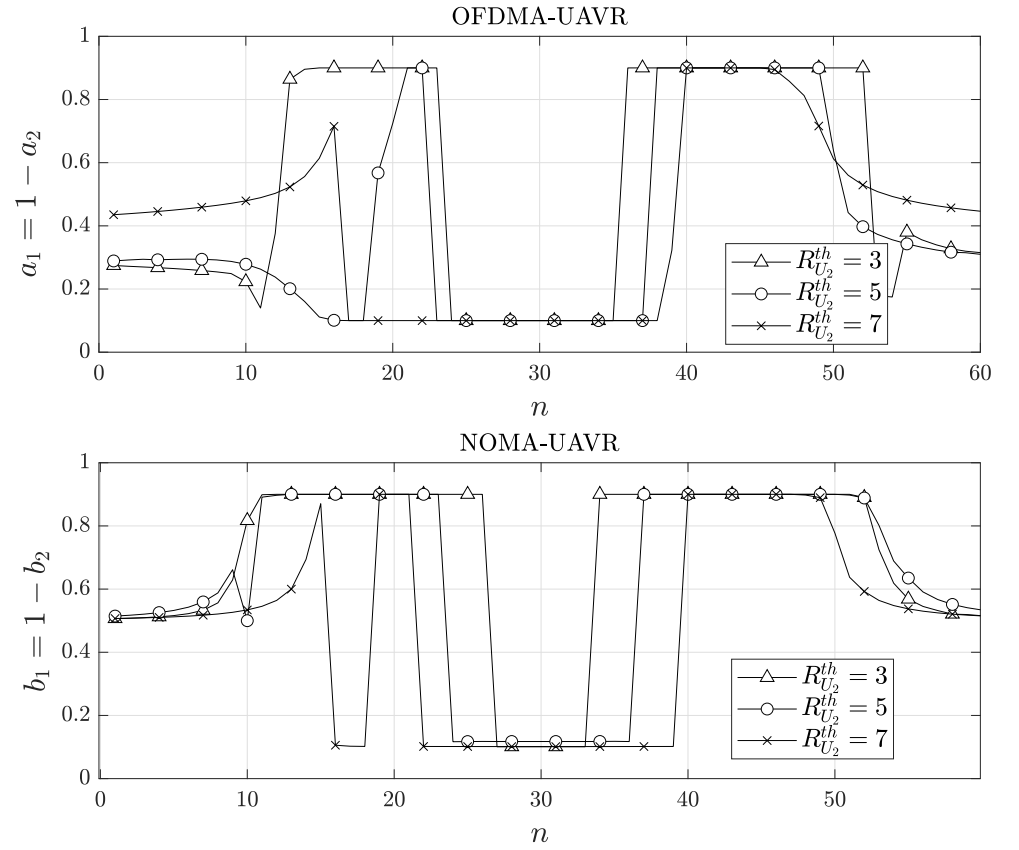


Figure 6. The allocation parameter for resources under varying $R_{U_2}^{\text{th}}$ values.

5.3. Analysis of instantaneous rate and sum data rate of each user

Figure 7 examines each user's optimal patterns in the instantaneous rate. The instantaneous rate is positive during the ECP and equal to zero during the rest phases. The instantaneous rate of U_1 receives high values at the beginning and end of the ECP, while the instantaneous rate of U_2 receives elevated values in the middle of the ECP. These patterns can be elucidated by referring to the outcomes regarding the flight trajectory of R , transmission power levels, and \mathbf{a} (or \mathbf{b}). When $R_{U_2}^{\text{th}}$ increases, the instantaneous rate of U_2 for each time slot becomes higher; moreover, the high-rate region of U_2 expands on both sides of the n axis, while the high-rate region of U_1 follows the inverse trend.

Figure 8 presents the trend of the optimal sum data rate for x_1 of U_1 and the optimal sum data rate for x_2 of U_2 . The purpose of our proposed algorithms is to maximize the system total data rate; however, Fig. 8 shows that the obtained efficient solution using the proposed algorithm aims to maximize the sum data rate of U_1 while guaranteeing the required sum data rate of U_2 . This is a reasonable result due to the disadvantageous position of U_2 . Comparing OFDMA-UAVR and NOMA-UAVR protocols, we realize that the OFDMA-UAVR protocol outperforms the NOMA-UAVR protocol at very low or very high values for $R_{U_2}^{\text{th}}$ whereas the NOMA-UAVR protocol outperforms the OFDMA-UAVR protocol at medium values for $R_{U_2}^{\text{th}}$ is medium (such as $R_{U_2}^{\text{th}} = 5$ or $R_{U_2}^{\text{th}} = 6$). These results emphasize the benefits of the NOMA-UAVR protocol in providing fair communication service for the multi-user system.

6. Conclusions

In this paper, we proposed algorithms to solve the system sum data rate maximization problem of a UAV-based relaying two-user system for two multiple access techniques, OFDMA and NOMA. Our proposed algorithms aim to guarantee service for the far user while maximizing the sum data rate for both users. By applying the SCO and BCGD

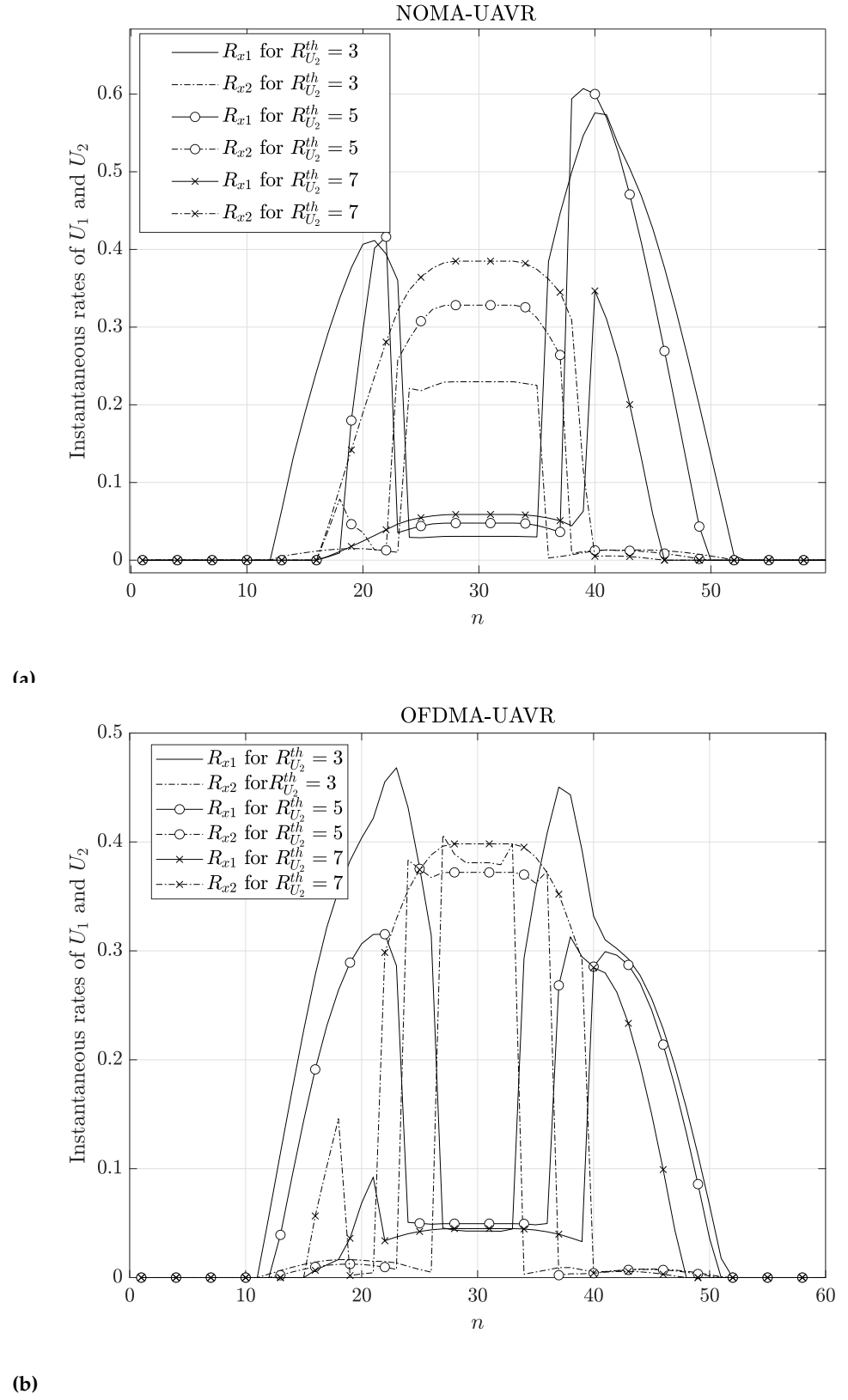


Figure 7. The instantaneous rate at each user for (a) NOMA-UAVR and (b) OFDMA-UAVR protocols with different values of $R_{U_2}^{\text{th}}$.

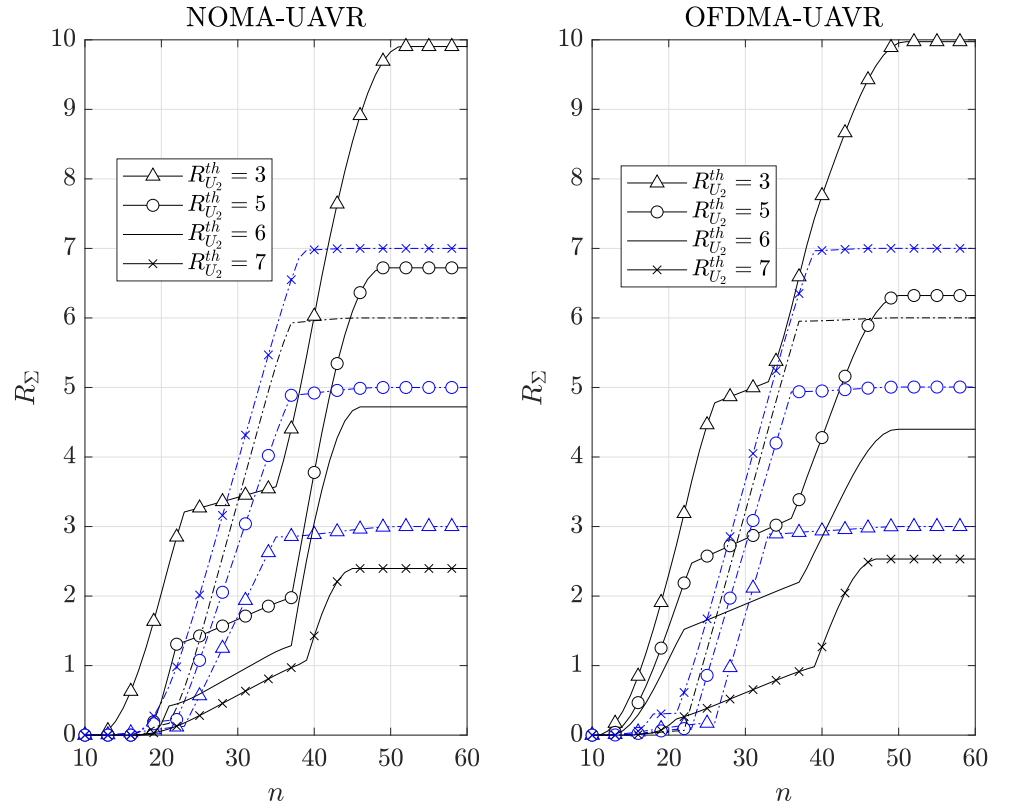


Figure 8. The optimal sum-rate at each user under varying of $R_{U_2}^{th}$ values.

techniques, the proposed algorithms optimized the UAV's flight trajectory, factors of resource allocation, and transmission powers. The numerical results confirmed that the system sum data rate significantly improved coverage. Furthermore, the optimal patterns in critical parameters, such as transmitted powers from GBS, the flight path and velocity of the UAV, and the resource allocation ratio, were revealed. Notably, the UAV tends to fly near or stay in specific areas, allowing efficient communication between the source and each user. The proposed algorithms tend to guarantee the minimum required sum data rate at the further destination user and maximize the sum data rate at the closer destination user. Finally, the obtained results demonstrate that the NOMA-UAVR protocol outperforms the OFDMA-UAVR protocol for the fair user-service scenario, whereas the OFDMA-UAVR protocol outperforms the NOMA-UAVR protocol in maximizing the system sum-rate for very low or very high required sum-rate rate for the far user.

Acknowledgments

This study is supported by the Research Fund of Hanoi University of Industry and thanks to Dr.Tuan Van-Phu, who supported us during the process.

Conflicts of Interest: Declare conflicts of interest or state "We wish to confirm that there are no known conflicts of interest associated with this paper. We confirm that the manuscript has been read and approved by all named authors and that there are no other persons who satisfied the criteria for authorship but are not listed. We further confirm that the order of authors listed in the manuscript has been approved by all of us".

Author Contributions: Building model, analysis, and writing—original draft preparation Thuc Kieu-Xuan; Building algorithms, performing experiments, and validation-Supervision Anh Le-Thi; All authors have read and agreed to the published version of the manuscript.

Abbreviations

The following abbreviations are used in this manuscript:

BCGD	Block-coordinate gradient descent
DU	Destination user
GBS	Round base station
NOMA	Non-Orthogonal Multiple Access
OMA	Orthogonal Multiple Access
OFDMA	Orthogonal frequency division multiple access
SCO	Successive Convex Optimization
SIC	Successive Interference Cancellation
SINR	Signal-to-Interference and Noise Ratio
UAV	Unmanned aerial vehicles
UAVR	UAV relaying
UAVWC	UAV-assisted wireless communication

References

1. Vinogradov, E.; Sallouha, H.; De Bast, S.; Azari, M.M.; Pollin, S. Tutorial on UAV: A blue sky view on wireless communication. *arXiv preprint arXiv:1901.02306* **2019**.
2. Shen, T.; Ochiai, H. A UAV-Enabled Wireless Powered Sensor Network Based on NOMA and Cooperative Relaying With Altitude Optimization. *IEEE Open Journal of the Communications Society* **2021**, *2*, 21–34. <https://doi.org/10.1109/OJCOMS.2020.3042257>.
3. Michailidis, E.T.; Maliatsos, K.; Skoutas, D.N.; Vouyioukas, D.; Skianis, C. Secure UAV-aided mobile edge computing for IoT: A review. *IEEE Access* **2022**, *10*, 86353–86383.
4. Duong, T.Q.; Kim, K.J.; Kaleem, Z.; Bui, M.P.; Vo, N.S. UAV caching in 6G networks: A Survey on models, techniques, and applications. *Physical Communication* **2022**, *51*, 101532.
5. Liu, D.; Xu, Y.; Wang, J.; Chen, J.; Yao, K.; Wu, Q.; Anpalagan, A. Opportunistic UAV utilization in wireless networks: Motivations, applications, and challenges. *IEEE Communications Magazine* **2020**, *58*, 62–68.
6. Guo, Y.; Yang, P. The Effectiveness of Unmanned Aerial Vehicle (UAV) on Farmlands with Artificial Intelligence (AI) System. In Proceedings of the 2022 7th International Conference on Financial Innovation and Economic Development (ICFIED 2022). Atlantis Press, 2022, pp. 1664–1669.
7. Thi Tam, D.; Cao Nguyen, B.; Manh Hoang, T.; The Dung, L.; Vinh, N.V.; Kim, T.; Lee, W. Combining FD-UAV and NOMA technologies in IoT sensor network with millimeter-wave communications. *International Journal of Communication Systems* **2023**, p. e5492.
8. Greenberg, E.; Bar, A.; Klodzh, E. Los classification of UAV-to-ground links in built-up areas. In Proceedings of the 2019 IEEE International Conference on Microwaves, Antennas, Communications and Electronic Systems (COMCAS). IEEE, 2019, pp. 1–5.
9. Cui, Z.; Briso-Rodríguez, C.; Guan, K.; Güvenç, I.; Zhong, Z. Wideband air-to-ground channel characterization for multiple propagation environments. *IEEE Antennas and Wireless Propagation Letters* **2020**, *19*, 1634–1638.
10. Zhang, X.; Duan, L. Fast deployment of UAV networks for optimal wireless coverage. *IEEE Transactions on Mobile Computing* **2018**, *18*, 588–601.
11. Shahzadi, R.; Ali, M.; Khan, H.Z.; Naeem, M. UAV assisted 5G and beyond wireless networks: A survey. *Journal of Network and Computer Applications* **2021**, *189*, 103114.
12. Sun, Y.; Wang, T.; Wang, S. Location optimization and user association for unmanned aerial vehicles assisted mobile networks. *IEEE Transactions on Vehicular Technology* **2019**, *68*, 10056–10065.
13. Khan, S.K.; Naseem, U.; Sattar, A.; Waheed, N.; Mir, A.; Qazi, A.; Ismail, M. UAV-aided 5G network in suburban, urban, dense urban, and high-rise urban environments. In Proceedings of the 2020 IEEE 19th International Symposium on Network Computing and Applications (NCA). IEEE, 2020, pp. 1–4.
14. Liu, Y.; Yi, W.; Ding, Z.; Liu, X.; Dobre, O.; Al-Dhahir, N. Application of NOMA in 6G networks: Future vision and research opportunities for next generation multiple access. *arXiv preprint arXiv:2103.02334* **2021**.
15. Khan, W.U.; Jameel, F.; Jamshed, M.A.; Pervaiz, H.; Khan, S.; Liu, J. Efficient power allocation for NOMA-enabled IoT networks in 6G era. *Physical Communication* **2020**, *39*, 101043.
16. Liu, Y.; Yi, W.; Ding, Z.; Liu, X.; Dobre, O.A.; Al-Dhahir, N. Developing NOMA to Next Generation Multiple Access: Future Vision and Research Opportunities. *IEEE Wireless Communications* **2022**.
17. Le, T.A.; Kong, H.Y. Evaluating the performance of cooperative NOMA with energy harvesting under physical layer security. *Wireless Personal Communications* **2019**, *108*, 1037–1054.
18. New, W.K.; Leow, C.Y.; Navaie, K.; Sun, Y.; Ding, Z. Application of NOMA for cellular-connected UAVs: Opportunities and challenges. *Science China Information Sciences* **2021**, *64*, 1–14.
19. Do, D.T.; Nguyen, T.T.T.; Nguyen, T.N.; Li, X.; Voznak, M. Uplink and downlink NOMA transmission using full-duplex UAV. *IEEE Access* **2020**, *8*, 164347–164364.
20. Zeng, Q.; Zhang, Z. The full-duplex device-to-device security communication under the coverage of unmanned aerial vehicle. *KSII Transactions on Internet and Information Systems (TIIS)* **2019**, *13*, 1941–1960.

21. Kumar, V.; Ding, Z.; Flanagan, M.F. On the Effective Rate of NOMA in Underlay Spectrum Sharing. *IEEE Transactions on Vehicular Technology* **2021**, *70*, 12220–12225. 467
22. Van Phu, T.; Kong, H.Y. Secrecy sum rate maximization for UAV-aided NOMA communication systems. *Annals of Telecommunications* **2022**, *77*, 127–138. 468
23. Wang, N.; Li, F.; Chen, D.; Liu, L.; Bao, Z. NOMA-based Energy-Efficiency optimization for UAV enabled space-air-ground integrated relay networks. *IEEE Transactions on Vehicular Technology* **2022**, *71*, 4129–4141. 469
24. Yang, Z.; Chen, M.; Liu, X.; Liu, Y.; Chen, Y.; Cui, S.; Poor, H.V. AI-driven UAV-NOMA-MEC in next generation wireless networks. *IEEE Wireless Communications* **2021**, *28*, 66–73. 470
25. Hariz, H.M.; Sheikhzadeh, S.; Mokari, N.; Javan, M.R.; Abbasi-Arand, B.; Jorswieck, E.A. Ai-based radio resource management and trajectory design for pd-noma communication in irs-uav assisted networks. *arXiv preprint arXiv:2111.03869* **2021**. 471
26. Senadhira, N.; Durrani, S.; Zhou, X.; Yang, N.; Ding, M. Uplink NOMA for Cellular-Connected UAV: Impact of UAV Trajectories and Altitude. *IEEE Transactions on Communications* **2020**, *68*, 5242–5258. <https://doi.org/10.1109/TCOMM.2020.2995373>. 472
27. Li, Y.; Zhang, H.; Long, K.; Jiang, C.; Guizani, M. Joint Resource Allocation and Trajectory Optimization With QoS in UAV-Based NOMA Wireless Networks. *IEEE Transactions on Wireless Communications* **2021**, *20*, 6343–6355. <https://doi.org/10.1109/TWC.2021.3073570>. 473

Disclaimer/Publisher's Note: The statements, opinions and data contained in all publications are solely those of the individual author(s) and contributor(s) and not of MDPI and/or the editor(s). MDPI and/or the editor(s) disclaim responsibility for any injury to people or property resulting from any ideas, methods, instructions or products referred to in the content. 482